

A Feedforward Mechanism Mediated by Mechanosensitive Ion Channel PIEZO1 and Tissue Mechanics Promotes Glioma Aggression

Highlights

- *Drosophila* Piezo regulates cell proliferation and tissue stiffening of gliomas
- Human PIEZO1 is overexpressed in aggressive gliomas and predicts poor survival
- Piezo/PIEZO1 interacts with integrin-FAK signaling to regulate tumor stiffness
- PIEZO1 co-opts aberrant tissue mechanics to promote glioma aggression

Authors

Xin Chen, Siyi Wanggou, Ankur Bodalia, ..., Lu-Yang Wang, Xuejun Li, Xi Huang

Correspondence

xi.huang@sickkids.ca

In Brief

PIEZO1 is an ion channel that converts mechanical stimuli into cellular signaling. Here, Chen et al. perform multi-species studies to define a feedforward circuit mediated by PIEZO1 and tumor tissue mechanics to promote glioma growth.



A Feedforward Mechanism Mediated by Mechanosensitive Ion Channel PIEZO1 and Tissue Mechanics Promotes Glioma Aggression

Xin Chen,^{1,2} Siyi Wanggou,³ Ankur Bodalia,^{4,5} Min Zhu,^{1,6} Weifan Dong,^{1,2,7} Jerry J. Fan,^{1,2,7} Wen Chi Yin,^{1,7} Hyun-Kee Min,^{1,2,7} Malini Hu,¹ Diana Draghici,¹ Wenkun Dou,⁶ Feng Li,^{8,9} Fiona J. Coutinho,^{1,2} Heather Whetstone,^{1,2} Michelle M. Kushida,^{1,2} Peter B. Dirks,^{1,2,7} Yuanquan Song,^{8,9} Chi-chung Hui,^{1,7} Yu Sun,⁶ Lu-Yang Wang,^{4,5} Xuejun Li,³ and Xi Huang^{1,2,7,10,*}

¹Program in Developmental and Stem Cell Biology, The Hospital for Sick Children, Toronto, ON M5G 1X8, Canada

²Arthur and Sonia Labatt Brain Tumour Research Centre, The Hospital for Sick Children, Toronto, ON M5G 1X8, Canada

³Department of Neurosurgery, Xiangya Hospital, Central South University, Changsha, Hunan 410008, China

⁴Program in Neurosciences and Mental Health, The Hospital for Sick Children, Toronto, ON M5G 1X8, Canada

⁵Department of Physiology, University of Toronto, Toronto, ON M5S 1A8, Canada

⁶Department of Mechanical and Industrial Engineering, University of Toronto, Toronto, ON M5S 3G8, Canada

⁷Department of Molecular Genetics, University of Toronto, Toronto, ON M5S 3E1, Canada

⁸The Raymond G. Perelman Center for Cellular and Molecular Therapeutics, The Children's Hospital of Philadelphia, Philadelphia, PA 19104, USA

⁹Department of Pathology and Laboratory Medicine, University of Pennsylvania, Philadelphia, PA 19104, USA

¹⁰Lead Contact

*Correspondence: xi.huang@sickkids.ca

<https://doi.org/10.1016/j.neuron.2018.09.046>

SUMMARY

Alteration of tissue mechanical properties is a physical hallmark of solid tumors including gliomas. How tumor cells sense and regulate tissue mechanics is largely unknown. Here, we show that mechanosensitive ion channel Piezo regulates mitosis and tissue stiffness of *Drosophila* gliomas, but not non-transformed brains. PIEZO1 is overexpressed in aggressive human gliomas and its expression inversely correlates with patient survival. Deleting PIEZO1 suppresses the growth of glioblastoma stem cells, inhibits tumor development, and prolongs mouse survival. Focal mechanical force activates prominent PIEZO1-dependent currents from glioma cell processes, but not soma. PIEZO1 localizes at focal adhesions to activate integrin-FAK signaling, regulate extracellular matrix, and reinforce tissue stiffening. In turn, a stiffer mechanical microenvironment elevates PIEZO1 expression to promote glioma aggression. Therefore, glioma cells are mechanosensory in a PIEZO1-dependent manner, and targeting PIEZO1 represents a strategy to break the reciprocal, disease-aggravating feedforward circuit between tumor cell mechanotransduction and the aberrant tissue mechanics.

INTRODUCTION

Cells in biological tissues are exposed to mechanical forces, including hydrostatic pressure, shear stress, compressional

force, and tensional force. Young's modulus (unit in force/area, N/m², or Pascals, Pa) describes the amount of force required to deform a substance, and it is used to reveal stiffness reflecting tissue rigidity. In biological systems, tissue stiffness varies greatly between organs, and between healthy and disease states of the same organ. As early as the Jin Dynasty (317–420 B.C.), Chinese medical writing by Dr. Hong Ge described breast cancer as being “hard as stone,” highlighting that alteration of mechanical properties is a physical hallmark of solid tumors. In certain regions, solid tumor tissues are stiffer than their non-transformed counterparts due to uncontrolled cell proliferation within confined spaces, hyper-permeable blood vessels, insufficient lymphatic drainage, and increased deposition of extracellular matrix (ECM) proteins. Augmented tissue stiffness actively instructs malignant progression by regulating proliferation, invasion, apoptosis evasion, drug resistance, blood vessel formation, metabolism, and growth-promoting signaling pathways (Kai et al., 2016; Northey et al., 2017; Oudin and Weaver, 2016; Przybyla et al., 2016; Tung et al., 2015).

Glioma is the most common brain tumor and can be categorized as low to high grade (Grade I–IV), with Grade IV glioblastoma (GBM) being the most frequent and aggressive primary brain tumor in adults. The standard treatment for GBM includes surgery, chemotherapy, and irradiation, which is largely ineffective, and GBM patients face a median survival of less than 14 months. While normal brain tissue stiffness is typically lower than 200 Pa, it has been reported that human low- to high-grade gliomas (LGG and HGG) display gradual increase in tissue stiffness that ranges from 100 to 10⁴ Pa (Miroshnikova et al., 2016). In addition, the presence of fluidic and cystic tissue in tumors highlights that heterogeneous stiffness levels can develop at different tumor regions. Tumor cells sense the aberrant physical microenvironment and transduce mechanical



force into intracellular signaling. Integrins are heterodimeric transmembrane protein complexes formed by α and β subunits. While the extracellular domain of integrins interacts with ECM proteins such as Collagens, Laminins, and Tenascin, their cytoplasmic domain complexes with scaffold proteins including Talin and Paxillin, and kinases such as focal adhesion kinase (FAK) and Src. These interactions allow transmission of environmental mechanical cues to control focal adhesion and cytoskeleton assembly, and activate integrin-dependent intracellular kinase signaling to regulate cell adhesion, motility, proliferation, survival, and differentiation (Kim et al., 2011). The integrin-focal adhesion kinase signaling is hence recognized as a major mechanotransduction mechanism in tumor. Other components of the tumor mechanosensing machinery have been identified, such as Rho family GTPases (Pajic et al., 2015), nonmuscle myosin II (Aguilar-Cuenca et al., 2014), and the Hippo pathway (Yu and Guan, 2013). Modeling the altered environmental mechanics and stiffness using a hydrogel-based cell culture platform has revealed that glioma cells interact with the ECM to regulate its expression of the oncogenic microRNA miR18a (Rape et al., 2015). The complex physical environment and varying stiffness encountered by different areas of the glioma cells can modulate their migratory capacity (Rape and Kumar, 2014). Increased environmental stiffness can also promote glioma cell proliferation by spatially and biochemically amplifying epidermal growth factor receptor (EGFR) signaling (Umesh et al., 2014). Furthermore, tumor tissue stiffness can be influenced by physiological state of the host, and obesity-induced interstitial fibrosis promotes breast cancer malignancy through altering mammary ECM mechanics (Seo et al., 2015). Therefore, a large body of evidence has reported aberrant tissue mechanics and its functional impact in tumor. However, our knowledge of tumor mechanosensation and mechanotransduction remains rudimentary. Cell surface sensors and transducers that directly perceive tissue mechanics to regulate tumor aggression remain to be fully defined.

The PIEZO transmembrane proteins are evolutionarily conserved ion channels that are intrinsically mechanosensitive (Murthy et al., 2017; Volkens et al., 2015; Wu et al., 2017). Physical force-induced membrane tension opens PIEZO channel to allow permeation of cations including sodium, potassium, and calcium (Cox et al., 2016; Lewis and Grandl, 2015). *Drosophila* Piezo regulates mechanosensory nociception (Kim et al., 2012) and gut stem cell differentiation (He et al., 2018), and its mammalian orthologs PIEZO1 and PIEZO2 convert mechanical stimuli to electrical and chemical signaling to regulate a multitude of physiological processes such as touch (Ranade et al., 2014b), proprioception (Chesler et al., 2016; Woo et al., 2015), respiration (Nonomura et al., 2017), urinary osmoregulation (Martins et al., 2016), blood flow (Li et al., 2014; Ranade et al., 2014a; Wang et al., 2016), epithelial homeostasis (Eisenhoffer et al., 2012; Gu-dipaty et al., 2017), axon growth (Koser et al., 2016), and cardiovascular homeostasis (Rode et al., 2017). Interestingly, PIEZO1 forms a mechanosensitive ion channel in a breast cancer cell line, while PIEZO2 was shown to regulate RhoA, actin cytoskeleton, and the motility of breast cancer cells *in vitro* (Li et al., 2015; Pardo-Pastor et al., 2018). However, it is unknown whether and

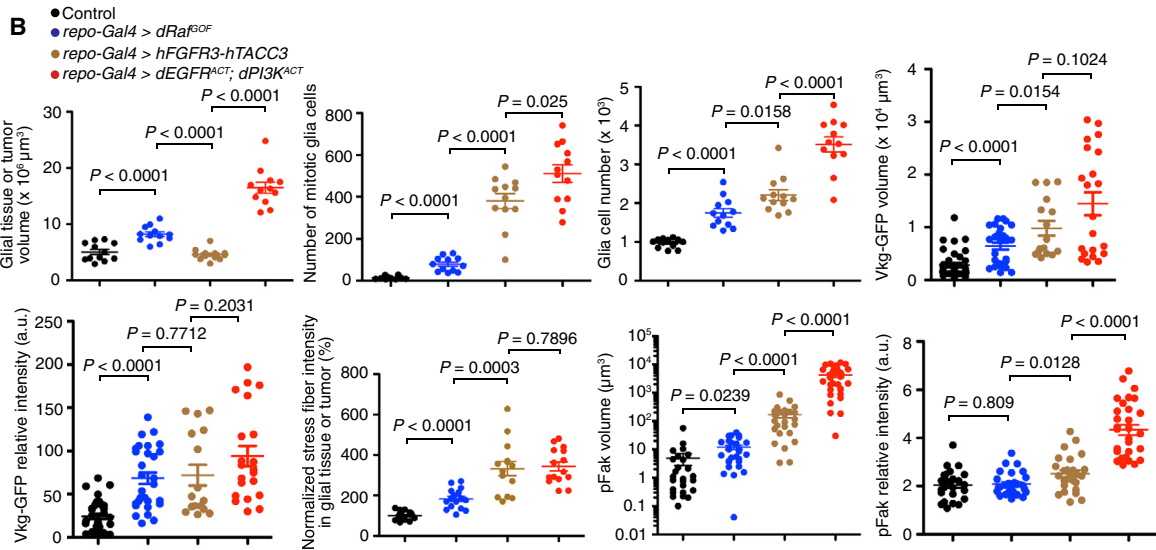
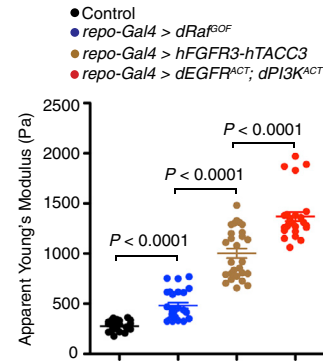
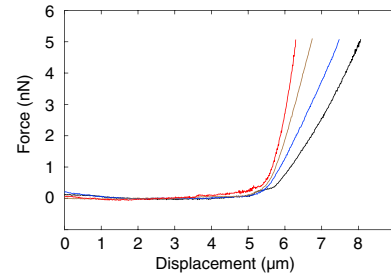
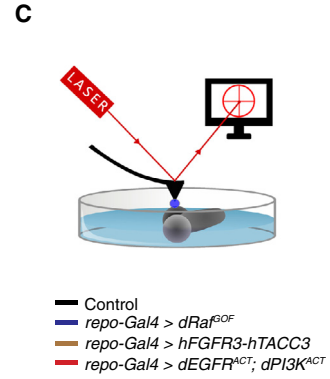
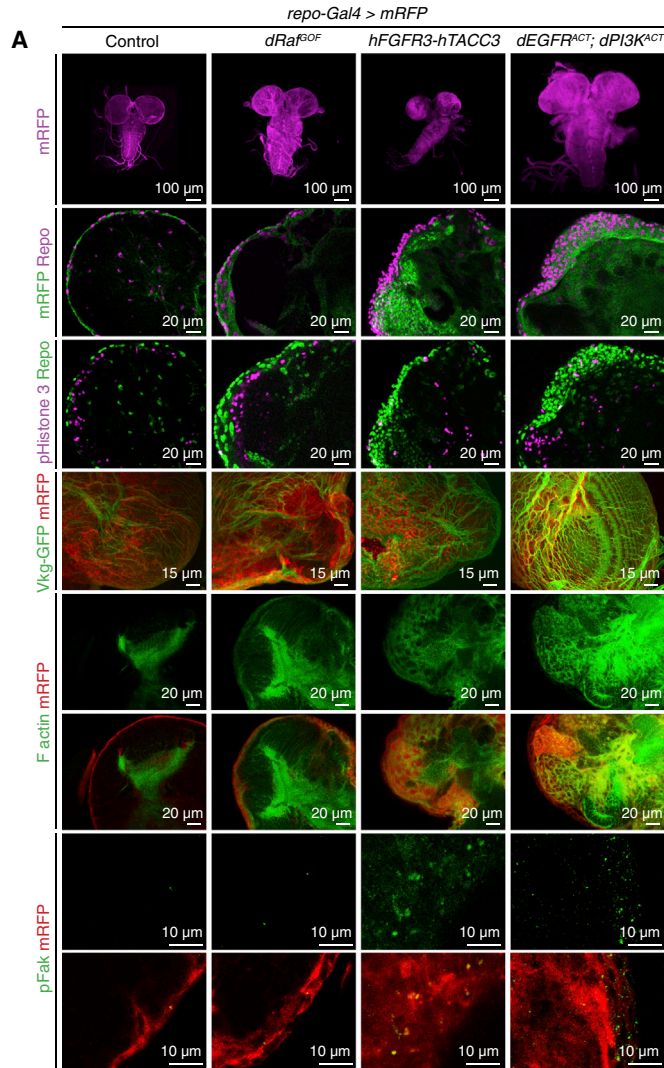
how PIEZO regulates *in vivo* tumorigenesis, whether tumors develop a heightened dependency on PIEZO for its malignant growth compared to non-transformed tissue, and whether the aberrant mechanical environment in tumors interplays with and hijacks the mechanosensory function of PIEZO to promote malignancy.

Here, we address these knowledge gaps by establishing multiple *Drosophila* models of gliomas and performing multi-species studies to define the functions of *Drosophila*, mouse, and human PIEZO in tumor. We discover that PIEZO channels play an evolutionarily conserved role to interact with integrin-FAK signaling to promote tissue stiffening and tumor cell proliferation. Moreover, the stiffer mechanical environment up-regulates PIEZO1 expression to further elevate tumor tissue mechanosensation to aggravate glioma progression. We identify a feedforward mechanosensory circuit in which PIEZO1 iteratively interacts with glioma tissue mechanics to promote malignant progression, and propose that targeting mechanosensitive ion channel-mediated tissue stiffening may have broad applicability across different tumor types driven by distinct oncogenic mutations.

RESULTS

Establish *Drosophila* Models of Low- and High-Grade Gliomas with Graded Increase of Tissue Stiffness

To determine how solid tumors sense and transduce tissue mechanics, we first established *Drosophila* glioma models that display tissue stiffening and facilitate genetic study to identify stiffness regulators *in vivo*. Activating genetic alterations in *BRAF* is common in LGGs (Penman et al., 2015). *FGFR-TACC* (transforming acidic coiled-coil containing protein) gene fusions are among the most common chromosomal aberrations in human cancers, and *FGFR3-TACC3* fusions were identified in 3% of GBM (Parker et al., 2013; Singh et al., 2012). Genetic gain and mutational activation of the EGFR and phosphatidylinositol-3 kinase (PI3K) pathways is found in over 40% of GBMs (Agnihotri et al., 2013). Using the glia cell-specific driver *repo-Gal4* to express mRFP and constitutively active *Drosophila* Raf (*dRaf^{GOF}*), human *FGFR3-TACC3* fusion gene (*hFGFR3-hTACC3*) (Frattini et al., 2018), or constitutively active *Drosophila* EGFR and PI3K (*dEGFR^{ACT}*; *dPI3K^{ACT}*) (Read et al., 2009), we established fly gliomas that show features of human LGGs to HGGs, including gradual increase in the number of pHistone3⁺; mRFP⁺ mitotic glia cells, the number of Repo⁺; mRFP⁺ total glia cells, and aberrantly enlarged brain tissues due to glial over-growth (Figures 1A and 1B). These tumors display increased deposition of the ECM protein Collagen IV marked by Vkg-GFP, enhanced intracellular contractility marked by Phalloidin (F actin) staining, and augmented Fak activation marked by phosphorylated Fak (Fak-pY397) (Figures 1A and 1B). These tumor cell-autonomous and extracellular changes suggest that these gliomas may develop aberrantly increased tissue stiffness. To directly determine tissue stiffness, we performed atomic force microscopy (AFM) indentation experiments. The AFM cantilever with spherical tip was brought in contact with and indented the brain tissue. The deflection of the cantilever was reflected by the laser spot position change that was



(legend on next page)

captured by a position-sensitive detector. Therefore, the slope of the indentation curve indicates the stiffness of the brain tissue. We found that fly gliomas driven by *dRaf^{GOF}*, *hFGFR3-hTACC3*, or *dEGFR^{ACT}*; *dPI3K^{ACT}* developed graded increase of tissue stiffness compared with non-transformed brains (Figures 1C and S1A), mimicking the gradual tissue stiffening in human LGGs to HGGs (Miroshnikova et al., 2016). Therefore, we established genetically tractable *Drosophila* models of gliomas that allow identification of molecular sensors and transducers of tissue mechanics in the tumors.

dPiezo Is Required for Proliferation and Stiffening of *Drosophila* Gliomas, but Not Normal Glial Tissue

Drosophila Piezo (dPiezo) forms mechanosensitive cation channels in sensory neurons to perceive noxious mechanical stimulation and regulate nociception (Kim et al., 2012), and it senses microenvironmental mechanical cues to regulate gut stem cell differentiation (He et al., 2018). Whether dPiezo functions in oncogenically transformed cells, however, is unknown. In our *Drosophila* genetic study, we used multiple mutant lines. *dPiezo^{KO}* refers to the global knockout for dPiezo (Kim et al., 2012). *RNAi-dPiezo^{KK}*, *RNAi-dPiezo^{GD}*, and *RNAi-dPiezo^{NI}* are three *Drosophila* lines that express different RNAi sequences, which target various regions of the *dPiezo* transcript, under UAS control. *repo-Gal4* simultaneously drives the expression of oncogenes and RNAi, which results in tumor-specific knockdown of dPiezo. We note that, as we perform genetic interaction studies, the choice for using a specific *RNAi-dPiezo* line or the *dPiezo^{KO}* line was determined by which chromosomes the various transgenes, including *RNAi-dPiezo*, *dPiezo^{KO}*, integrin pathway genes, *Drosophila* Piezo, mouse Piezo1, and human PIEZO1, are on. Suitable combinations of alleles were used to establish the desired compound mutant fly lines.

Strikingly, we found that global dPiezo knockout significantly reduced tumor volume and decreased the number of mitotic and total glia cells in gliomas driven by *dEGFR^{ACT}*; *dPI3K^{ACT}* (Figures 2A–2C). *repo-Gal4*-driven tumor-specific RNAi knockdown of dPiezo also suppressed the growth of fly gliomas driven by *dEGFR^{ACT}*; *dPI3K^{ACT}*, *hFGFR3-hTACC3*, or *dRaf^{GOF}* (Figures 2A–2C), suggesting that dPiezo plays a cell-autonomous role.

We asked whether dPiezo is required for the proliferation of non-transformed glia cells. Interestingly, dPiezo did not appear to be expressed in normal glial tissue (Figure 2D). In line with the lack of glial expression, dPiezo knockout had no discernible impact on the volume of glial tissue or glia cell mitosis (Figure 2E). Importantly, genetic deletion of dPiezo significantly reduced tissue stiffness in the three different glioma models but had no impact on stiffness of normal brains (Figure 2F). These findings demonstrate that *Drosophila* gliomas driven by various oncogenic mutations develop tumor-specific dependency on the mechanosensitive channel dPiezo to regulate tissue stiffening and malignant growth *in vivo*.

dPiezo Genetically Interacts with Integrin Signaling to Promote Tissue Stiffening and Glioma Aggression

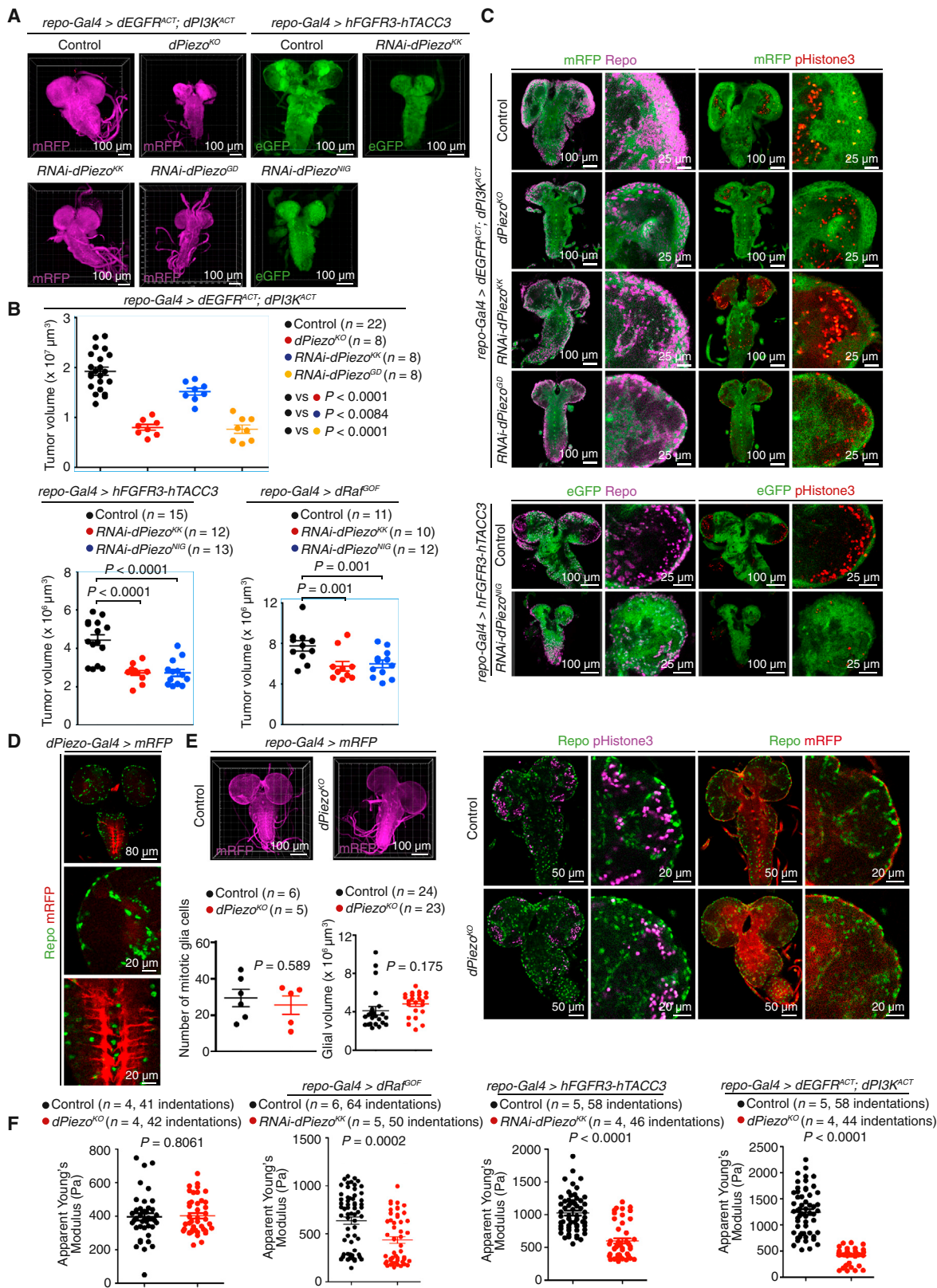
Next, we sought to determine the mechanism by which dPiezo regulates glioma growth. Since integrins physically interact with ECM proteins to relay mechanical cues into intracellular kinase signaling, we asked whether dPiezo-mediated signaling genetically interacts with integrin-dependent kinase signaling in the tumor. We expressed multiple components of the integrin pathway, including *Drosophila* α and β integrins (Mew and Mys), Paxillin, and Integrin-linked kinase (Ilk) in dPiezo-deficient gliomas. Notably, expressing the structural proteins or kinase in the integrin pathway significantly increased the numbers of mitotic glia cells and total glia cells, and rescued tumor growth in dPiezo-deficient gliomas driven by constitutively active EGFR and PI3K or the FGFR3-TACC3 fusion oncogene (Figures 3A and 3B). Activating integrin signaling also significantly increased tissue stiffness in the dPiezo-deficient, FGFR3-TACC3-driven glioma (Figure 3B). Interestingly, increasing production of ECM protein from the tumor cells by expression of *Drosophila* Laminin A (LanA, ortholog for human Laminin A) or *kkv* (ortholog for human hyaluronic acid synthases that produce hyaluronic acid, a key ECM constituent) rescued the growth of tumors with dPiezo knockout (Figure S1B), suggesting that tissue mechanics can be sensed and transduced by molecules in addition to dPiezo. Taken together, these results show that dPiezo genetically interacts with integrin signaling to reinforce tissue stiffening and promote glioma aggression.

Figure 1. *Drosophila* Gliomas Recapitulate Features of Human Low- to High-Grade Gliomas

(A) Immunofluorescence micrographs show the brain lobes and ventral nerve cords of late third instar *Drosophila* larvae. Glia-specific *repo-Gal4*-driven expression of mRFP and gain-of-function *Drosophila* Raf (*dRaf^{GOF}*), human fusion oncogene *hFGFR3-hTACC3*, or constitutively active *Drosophila* EGFR and PI3K (*dEGFR^{ACT}* and *dPI3K^{ACT}*) results in graded increase in mRFP⁺ glial tissue or tumor volume, number of Repo⁺ glia cells, number of pHistone3⁺ mitotic glia cells, expression of Vkg-GFP⁺ Collagen IV, F-actin⁺ stress fibers, and pFak⁺ cells that express activated focal adhesion kinase in the mRFP⁺ tumors. Note that 3D stacked images are shown for Vkg-GFP merged with mRFP.

(B) Quantifications of glial tissue or tumor volume, number of mitotic glia cells, number of total glia cells, Vkg-GFP, stress fiber, and pFak in non-transformed control brains and gliomas. Vkg-GFP and pFak signals in mRFP⁺ tumors were measured in various defined volumes of 10⁵ μm^3 mRFP⁺ tumors to generate volume and intensity values. For control, *repo-Gal4 > dRaf^{GOF}*, *repo-Gal4 > hFGFR3-hTACC3*, and *repo-Gal4 > dEGFR^{ACT}*; *dPI3K^{ACT}*, n = 12, 12, 12, 12 for glial tissue or tumor volume; n = 12, 12, 12, 12 for number of mitotic glia cells; n = 12, 12, 12, 12 for glia cell number; n = 17 (37 data points), 13 (29 data points), 8 (16 data points), 11 (21 data points) for Vkg-GFP volume; n = 17 (34 data points), 13 (29 data points), 8 (16 data points), 11 (21 data points) for Vkg-GFP relative intensity; n = 8 (18 data points), 8 (16 data points), 8 (14 data points), 8 (15 data points) for normalized stress fiber intensity in glial tissue or tumor; n = 7 (26 data points), 7 (28 data points), 7 (26 data points), 6 (30 data points) for pFak volume; n = 7 (26 data points), 7 (28 data points), 7 (26 data points), 6 (30 data points) for pFak relative intensity, respectively. a.u., arbitrary unit. Error bars, mean \pm SEM.

(C) Tissue stiffness in *Drosophila* gliomas and non-transformed brains measured by atomic force microscopy. The same amount of force results in less displacement in gliomas compared to non-transformed brains, revealing increased tissue stiffness in the tumors. For control, *repo-Gal4 > dRaf^{GOF}*, *repo-Gal4 > hFGFR3-hTACC3*, and *repo-Gal4 > dEGFR^{ACT}*; *dPI3K^{ACT}*, n = 3 (27 indentations), 3 (27 indentations), 3 (27 indentations), and 3 (27 indentations), respectively. Error bars, mean \pm SEM.



(legend on next page)

Evolutionarily Conserved dPiezo/PIEZO1 Function in Glioma Depends on Its Ion Conductance

PIEZO channels are large integral membrane proteins with more than 2,500 amino acids and at least 26 transmembrane domains (Ge et al., 2015; Saotome et al., 2018). Given their large intracellular domains, it remains to be determined whether PIEZO function in glioma depends on their ability to conduct ions or non-conductive protein-protein interaction. To address this question, in dPiezo knockout glioma we introduced tumor-specific expression of wild-type human PIEZO1 (hPIEZO1), wild-type mouse Piezo1 (mPiezo1), a gain-of-function mouse Piezo1 (mPiezo1-TriM) in which the mutations (E2133D, D2139E, and D2144E) result in a very slowly inactivating mechanically activated current (unpublished data), and a mutant form of mouse Piezo1 (mPiezo1-2336-Myc) in which the Myc tag insertion in the last extracellular loop renders the channel non-conducting without affecting its expression or trafficking to the membrane (Coste et al., 2015). Importantly, we found that all but mPiezo1-2336-Myc significantly rescued glioma growth and increased tissue stiffness in gliomas with dPiezo knockout (Figure 3C). Expressing mPiezo1-2336-Myc further suppressed glioma growth and decreased tissue stiffness in the dPiezo knockout background (Figure 3C), suggesting that the non-conducting protein may affect a tumor-promoting mechanism that is parallel to dPiezo signaling. In order to confirm that mPiezo1-2336-Myc can traffic to the cell surface, we performed Myc immunostaining to determine the localization in fly glioma cells. We found that Myc signal overlaps with mCD8-GFP that marks plasma membrane (Figure S1C). Therefore, these results demonstrate that the function of dPiezo/PIEZO1 in regulating glioma growth is evolutionarily conserved, and illustrate that the channel function of PIEZO to permeate ions is critical to glioma malignancy.

PIEZO1 Is Overexpressed in Human Gliomas, Inversely Correlates with Patient Survival, and Regulates Tumor Growth

Having established the important function of dPiezo in regulating fly glioma growth, we investigated the expression and clinical significance of its orthologs, PIEZO1 and PIEZO2, in human gliomas. We first performed “one to all” matrix correlation analysis in four TCGA glioma datasets containing 1,232 glioma samples to define *PIEZO1*-correlated genes. We calculated Pearson's correlation coefficient in 73,632 gene pairs that include *PIEZO1* from the four datasets, and identified a total of 345 genes as

PIEZO1 correlated (9 negatively correlated and 336 positively correlated). Next, we performed unsupervised hierarchical clustering using the TCGA GBM dataset ($n = 539$) and TCGA LGG-GBM dataset ($n = 702$). Interestingly, both datasets can be subdivided into three subgroups based on the level of *PIEZO1* expression (*PIEZO1* high, *PIEZO1* moderate, and *PIEZO1* low) (Figures 4A and S2). Compared with normal brain tissue, all the histological subtypes of gliomas, except oligodendroglioma, show *PIEZO1* overexpression (Figures 4A and S3A). *PIEZO1* is upregulated in HGGs (WHO Grade 3 and 4) compared with LGGs (WHO Grade 2) (Figure 4A), and high *PIEZO1* expression tends to be associated with astrocytoma component (Figures 4A and S3A). IDH mutation, glioma CpG island methylator (G-CIMP) phenotype, and 1p/19q co-deletion are important molecular biomarkers that guide prognostication and treatment. Interestingly, in these four independent TCGA datasets, we found that *PIEZO1* is decreased in IDH mutant gliomas including LGGs and GBMs (Figures 4A and S3B), and in the TCGA LGG dataset, *PIEZO1* expression is elevated in 1p/19q non-co-deletion group, where it is low and high in gliomas with G-CIMP phenotype and non-G-CIMP phenotypes, respectively (Figures 4A and S3B). Next, we performed *PIEZO1* immunohistochemistry using a panel of human glioma tumor tissues including LGGs, primary GBMs, and recurrent GBMs. We found that most tumor samples displayed positive *PIEZO1* expression (Figure S3C), consistent with the fact that *PIEZO1* mRNA upregulation is widespread across LGGs and GBMs (Figure 4A). Importantly, in this panel of tumor tissues, we detected minimal *PIEZO1* protein expression in a grade II oligodendroglioma that has IDH1 mutation and 1p/19q co-deletion (Figure S3C). This finding further supports our bioinformatics data (Figure 4A).

Since the expression of *PIEZO1* of IDH mutant glioma is lower than that of the IDH wild-type glioma and IDH mutation establishes a glioma hyper-methylation phenotype, we asked whether *PIEZO1* promoter is hyper-methylated in IDH mutant glioma. We investigated 38 probes spanning *PIEZO1* promoter in chromosome 16, and marked *PIEZO1* promoter region by using chromatin immunoprecipitation sequencing (ChIP-seq) peak signal of H3K4me3 (Figure S4A). Markedly, we found that the DNA domain spanning *PIEZO1* promoter and the upstream 8,000 bp of *PIEZO1* transcription start site (TSS) are hyper-methylated in IDH mutant glioma (Figure S4A). Importantly, the methylation status of most of these probes negatively correlates with *PIEZO1* mRNA expression (Figure S4A). The methylation status of

Figure 2. Mechanosensitive Ion Channel dPiezo Is Required for Proliferation and Tissue Stiffening in Gliomas, but Not Non-transformed Brains

(A) Immunofluorescence micrographs show the brain lobes and ventral nerve cords of late third instar *Drosophila* larvae. Global dPiezo knockout or *repo-Gal4*-driven tumor-specific dPiezo knockdown inhibits the growth of gliomas driven by dEGFR^{ACT}, dPI3k^{ACT} or hFGFR3-hTACC3. *dPiezo*^{KO} refers to the global knockout for dPiezo. *RNAi-dPiezo*^{KK}, *RNAi-dPiezo*^{GD}, and *RNAi-dPiezo*^{NI} are three lines that express different RNAi that target various regions of the *dPiezo* transcript under UAS control.

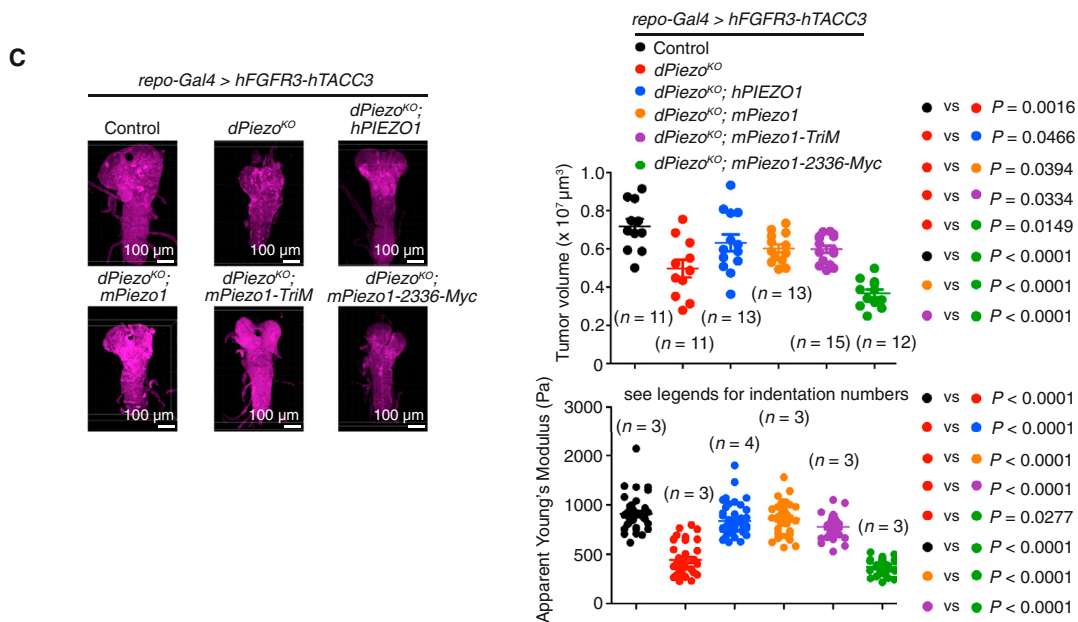
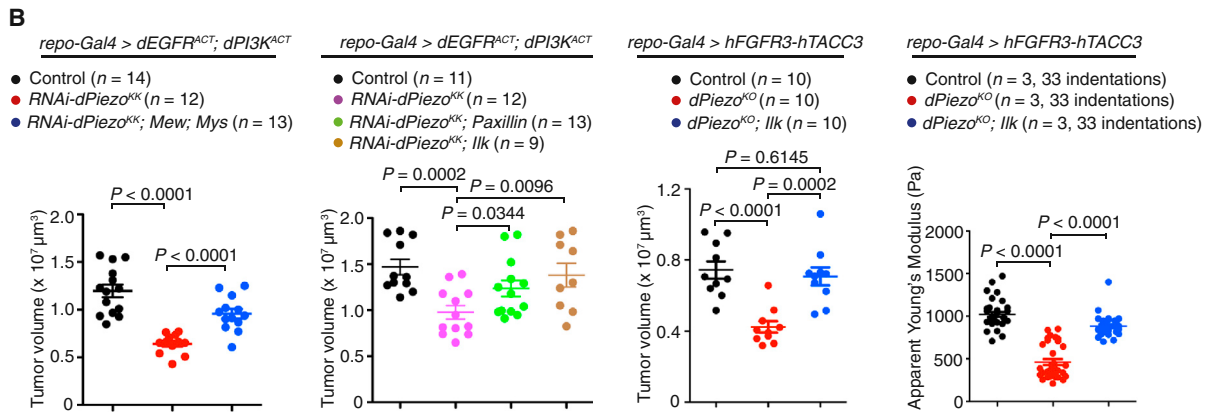
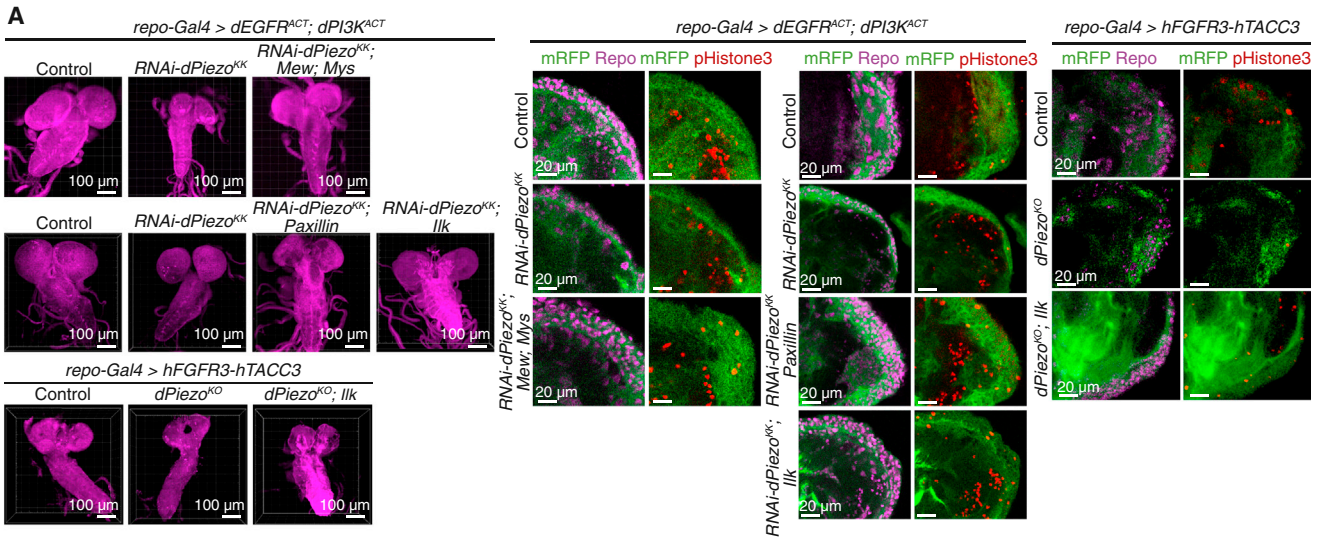
(B) Quantifications of volumes of control tumors and dPiezo-deficient gliomas driven by dEGFR^{ACT}, dPI3k^{ACT}, hFGFR3-hTACC3, or dRaf^{GOF}. Error bars, mean \pm SEM.

(C) Genetic deletion of dPiezo shows decreased glioma cell mitosis and the number of total glioma cells compared to control tumors.

(D) *Piezo-Gal4*-driven mRFP expression is not detected in normal *Repo*⁺ glia cells.

(E) Global dPiezo knockout does not overtly affect glial tissue volume, glia cell mitosis, or the number of glia cells in non-transformed brains compared to the wild-type controls. Error bars, mean \pm SEM.

(F) Quantifications of tissue stiffness measured by atomic force microscopy with genetic deletion of dPiezo in non-transformed brains and gliomas driven by different oncogenic mutations. Error bars, mean \pm SEM.



(legend on next page)

regions spanning *PIEZO1* promoter demonstrates significant differences between IDH mutant and IDH wild-type gliomas (Figure S4B), and for most regions in the upstream of *PIEZO1* TSS containing the promoter, IDH mutant gliomas also showed a significantly hyper-methylated phenotype (Figure S4B). These data suggest that the generally more aggressive IDH wild-type gliomas are epigenetically more poised to upregulate *PIEZO1* at the transcription level. Consistent with our findings that high *PIEZO1* expression associates with these molecular markers predictive of worse prognosis (IDH wild-type, 1p/19q non-co-deletion, non-G-CIMP phenotype), Kaplan-Meier survival analysis for multiple human glioma datasets showed that patients with elevated *PIEZO1* expression displayed significantly worse overall survival (Figures 4B and S5A).

Next, we investigated whether human GBM cells display *PIEZO1*-dependent mechanosensitive ion channel activity. We developed a novel approach whereby our mechanical stimulation can precisely target cellular processes or cell soma, rather than the GBM cell as a whole. Given the delicate structure of cellular processes, we strategized to evoke mechanosensitive currents with brief applications of solution ejected from a glass pipette electrode under variable positive pressures, thus avoiding invasive contact with the processes and in turn maintaining their morphological structure and membrane integrity. Previous studies from the Patapoutian lab (Syeda et al., 2016) and the Gu lab (Jia et al., 2016) demonstrated *PIEZO* channel sensitivity to an osmotic gradient. Therefore, we performed whole-cell voltage-clamp recordings of mechanosensitive currents using both hypertonic and isotonic solutions for comparison. When brief puffs of solution were delivered under defined levels of pressure to the G532 GBM stem cells, we found that both isotonic and hypertonic solutions applied to the cellular processes reliably evoked mechanosensitive channel activity, whereas identical stimulation paradigms evoked little to no response from the soma of the same cells (Figure 4C). Importantly, hypertonic solution evoked significantly larger currents compared to isotonic solution (Figure 4C), consistent with the published studies that *PIEZO* channels can be modulated by osmotic gradient. The compartmentalized channel activity is reinforced by the immunostaining evidence showing *PIEZO1* localization at focal adhesion sites prominently clustered at the GBM stem cell processes (Figure 5C). The linear I-V relationship demonstrates that the mechanosensitive current displays non-selective cation channel properties as the reversal potential is near 0 mV (Figure S6A). Notably, the currents were abrogated by *PIEZO1* knockdown (Figure 4C), suggesting that *PIEZO1* is one of the primary ion channels that confer mechanosensitivity to the GBM stem cells.

Next, we sought to determine whether *PIEZO1* function is required for the growth of GBM cells and tumors. We used three human GBM cell lines (GS2, SF7225, and SF7881) cultured with serum, as well as three human GBM stem cell lines (G508, G532, and G411), which were established from mesenchymal GBM tumors and cultured under stem cell condition without serum (Pollard et al., 2009). G508 cells display amplifications in *CDK4*, *MDM4*, and *EGFR*, and loss of one copy of *PTEN*. G532 cells display amplification in *PDGFRA* and loss of one copy of *PTEN*. G411 cells display *EGFR* amplification. Remarkably, *PIEZO1* knockdown not only ablated the cellular response to mechanical force to permeate ions, but also suppressed the clonogenic growth of GBM cell lines (Figures 4D and 4E). Tumor sphere formation of GBM stem cell lines was abrogated by *PIEZO1* knockdown (Figure 4F). *PIEZO1* knockdown inhibited the *in vivo* growth of GBM and significantly prolonged the survival of mice bearing tumors with constitutive knockdown of *PIEZO1* (G532 or G411) compared to mice bearing control tumors (Figure 4H). Furthermore, we generated G411 GBM cells that can express *PIEZO1* short hairpin RNA (shRNA) in a doxycycline-dependent manner (Figures S7A and S7B). We treated the mice with doxycycline after tumor implantation and found that while the initial tumor growth was comparable between the control and doxycycline-treated mice, inducible *PIEZO1* shRNA expression significantly suppressed GBM tumor growth and prolonged mouse survival (Figures 4G and 4H), demonstrating that *PIEZO1* is required for glioma maintenance and progression once the tumors have formed. Intriguingly, interrogation of the TCGA Pan-Cancer dataset revealed that *PIEZO1* is overexpressed across multiple types of human tumors despite different tissue origins, including cancers in the brain, liver, thyroid, kidney, rectum, colon, head and neck, stomach, and prostate (Figure S5B), suggesting that *PIEZO1*-mediated mechanosensation may be a general mechanism employed by solid tumors. *PIEZO2* expression does not appear to enrich in specific subtypes of gliomas, and we found no correlation between *PIEZO2* expression and patient survival (Figure S6B). Taken together, these findings show that *PIEZO1* is overexpressed in the most aggressive human glioma types, and it confers both mechanosensitivity to permeate ions and growth advantage to the tumors.

PIEZO1 Localizes at Focal Adhesion to Regulate Its Assembly and Activation of Integrin Signaling

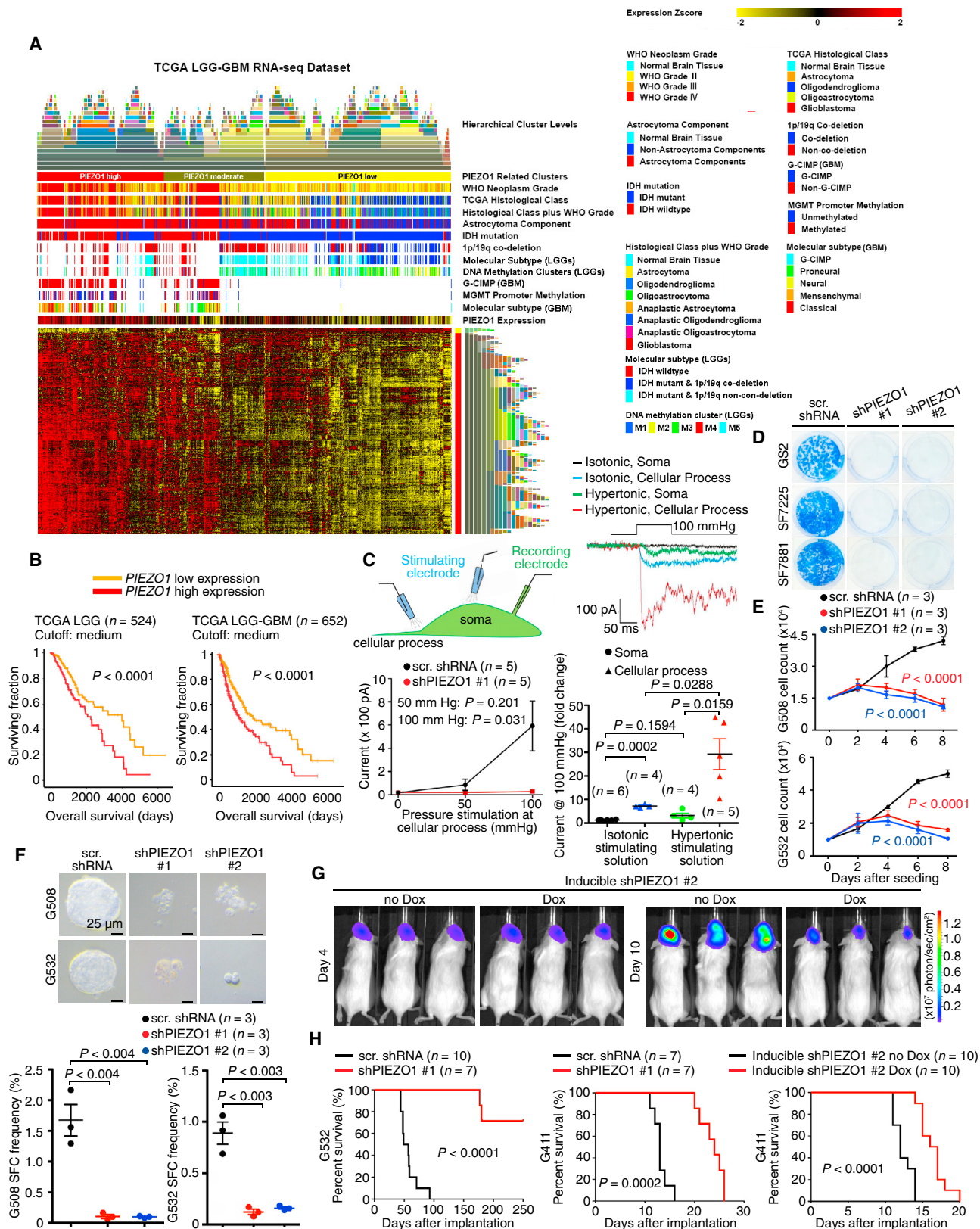
To explore the mechanisms by which *PIEZO1* regulates glioma malignancy, we performed DAVID functional enrichment analysis of the human glioma datasets to annotate *PIEZO1*-correlated genes. Noticeably, most of the significantly enriched pathways are related to tissue stiffness, including pathways of ECM

Figure 3. Evolutionarily Conserved PIEZO Function in Glioma Depends on Its Ion Conductance and Interacts with Integrin Signaling

(A) Immunofluorescence micrographs show the brain lobes and ventral nerve cords of late third instar *Drosophila* larvae. Tumor-specific expression of *Drosophila* α and β integrins (Mew and Mys), Paxillin, or Integrin-linked kinase (Ilk) in dPiezo-deficient gliomas increases tumor volume, mitosis, and the total number of tumor cells.

(B) Quantifications of tumor growth and tissue stiffness after activating integrin signaling in dPiezo-deficient gliomas. Error bars, mean \pm SEM.

(C) Fluorescence micrographs show the brain lobes and ventral nerve cords of late third instar *Drosophila* larvae. Gliia-specific expression of hPIEZO1, mPiezo1, or mPiezo1-TriM rescues tumor growth and increases tissue stiffness of hFGFR3-hTACC3-driven glioma with genetic knockout of the endogenous dPiezo. mPiezo1-2336-Myc, which cannot conduct ions, fails to rescue. Indentation numbers for Young's modulus measurements: control (38), dPiezoKO (36), dPiezoKO; hPIEZO1 (48), dPiezoKO; mPiezo1 (36), dPiezoKO; mPiezo1-TriM (28), dPiezoKO; mPiezo1-2336-Myc (36). Error bars, mean \pm SEM.



(legend on next page)

organization, collagen catabolic process, cell adhesion, integrin binding, actin cytoskeleton, focal adhesion, ECM-receptor interaction, and cellular response to mechanical stimulus (Figures 5A and 5C). Importantly, most *PIEZO1*-correlated genes can be projected into multiple pathways, suggesting that *PIEZO1* serves as a central functional node that integrates various regulators of a tissue stiffness-regulating molecular network (Figure 5B). These bioinformatic data prompted us to ask whether *PIEZO1* physically localizes to subcellular compartments in the tumor cells to facilitate its interaction with ECM and focal adhesion. Remarkably, we discovered that *PIEZO1* localizes to focal adhesions where integrin and FAK are activated in the GBM stem cells (Figure 5C). While control cells developed at their periphery elongated focal adhesions marked by the expression of Vinculin, FAK, activated $\beta 1$ integrin, and phosphorylated Paxillin (Tyr118), *PIEZO1* knockdown cells failed to assemble focal adhesion structures or activate the integrin-FAK pathway (Figures 5D–5F). The specificity of the *PIEZO1* antibody that we used was supported by RNAi-mediated (Figures 5D and 5F) and CRISPR-Cas9-mediated loss-of-function studies (Figure S8A). Interestingly, in our antibody validation experiment, after targeting exon 6 or 7 of *PIEZO1* using two different guide RNAs and establishing 24 single-cell clones of the HEK293T cells, we observed that most clones displayed strong reduction of *PIEZO1* protein expression (Figure S8A). Our finding suggests that homozygous *PIEZO1* knockout may affect the growth of the HEK293T cells, and we obtained heterozygous clones with *PIEZO1* deletion on one chromosome. The reduced western blotting protein band signal supports that the *PIEZO1* antibody we used is specific. In addition, to demonstrate that the focal adhesion phenotypes are not secondary to compromised cell viability, we performed immunostaining experiments at an earlier time point when there was no apparent reduction in viability in the *PIEZO1* knockdown cells. Under this circumstance, we still observed that *PIEZO1* knockdown led to strong defects in focal adhesion assembly and activation of the integrin-FAK pathway (Figures S8B–S8D). These findings are consistent with the genetic interaction between dPiezo and integrin-Fak pathway in *Drosophila* gliomas (Figures 3A and 3B). Collectively, our data demonstrate that in human LGGs and HGGs, despite being driven by divergent oncogenic mutations and signaling path-

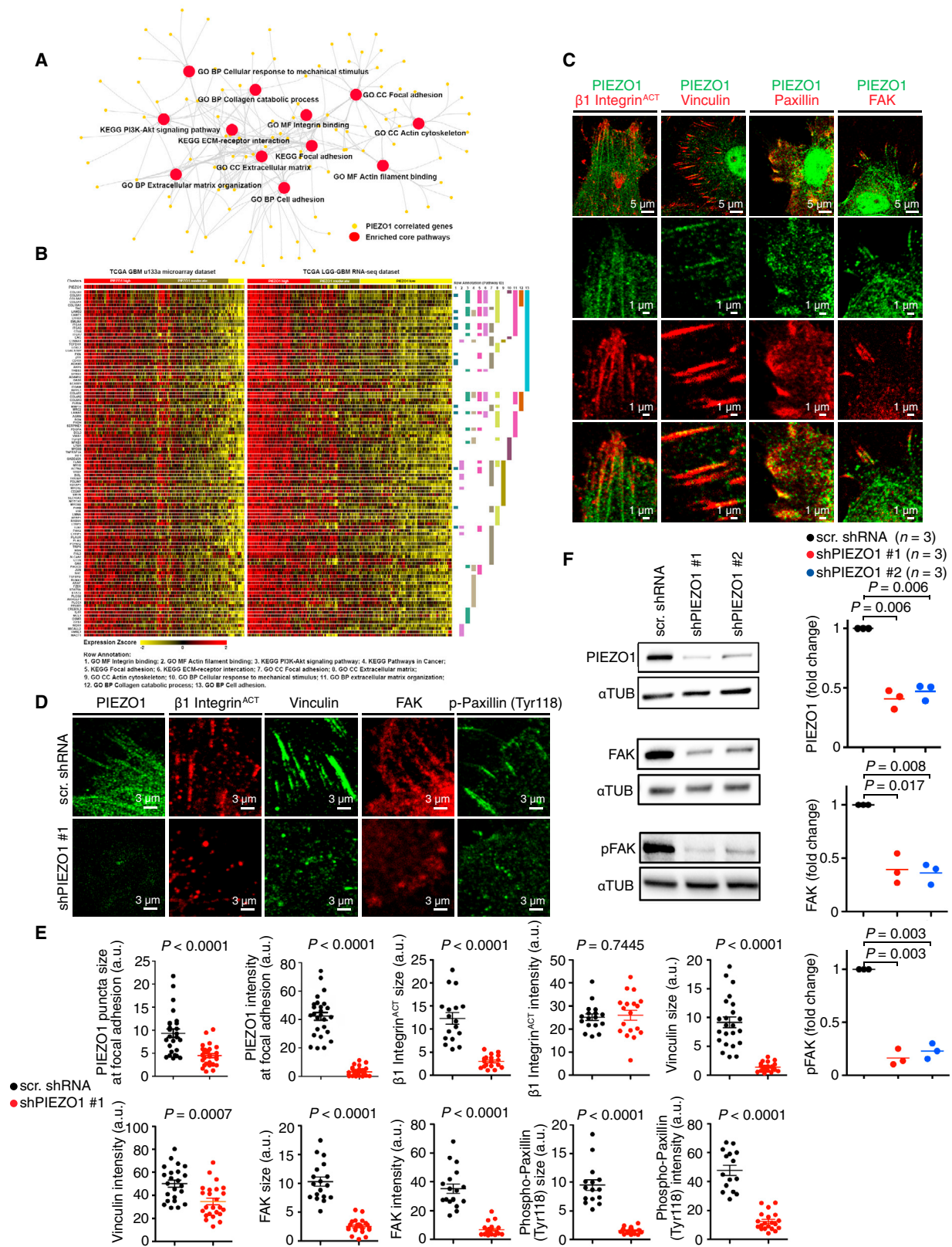
ways, and possibly arising from distinct brain regions, elevated *PIEZO1* expression is associated with active ECM remodeling, actin cytoskeleton organization, and focal adhesion-integrin signaling. Notably, the localization of *PIEZO1* at focal adhesions supports our electrophysiological data that GBM stem cells display prominent mechanosensitive ion channel activity only when their cellular processes were mechanically stimulated (Figure 4C). This spatially segregated *PIEZO1* channel activity promotes efficient assembly and signaling of focal adhesions, which serve as highly localized subcellular domains for *PIEZO1* to perceive mechanical stimuli at the cell surface. With a recent study reporting that *PIEZO2* channel generates calcium signals at focal adhesions to regulate stress fiber formation in a breast cancer cell line (Pardo-Pastor et al., 2018), our findings establish focal adhesions as central hubs where physical localization of *PIEZO* channels senses and integrates mechanical cues to regulate intracellular signaling in diverse cell types.

A Reciprocal *PIEZO1*-Dependent Feedforward Mechanism between Tissue Stiffening and Tumor Mechanotransduction

To unequivocally establish *PIEZO1* as the key regulator that senses microenvironmental stiffness and transduces the mechanical cue into growth-promoting signal, we cultured GBM stem cells in polyacrylamide hydrogels of various levels of stiffness (100–5,000 Pa), which encompass the stiffness range from normal human brain, LGGs to HGGs. The percentage of GBM stem cells undergoing active cell cycling and the total number of cells increased with stiffness. However, *PIEZO1* knockdown abrogated this stiffness-dependent tumor cell growth (Figures 6A–6D). Unexpectedly, we found that both the mRNA and protein levels of *PIEZO1* were upregulated by the increased environmental stiffness (Figures 6E and 6F). Next, we decided to determine the effect of activating the ion channel activity of endogenous *PIEZO1* by treating GBM cells with a specific *PIEZO1* agonist (Yoda1). We found that the GBM cells displayed comparable growth with or without Yoda1 treatment at all tested stiffness levels (Figure S8E), suggesting that while endogenous *PIEZO1* is necessary for GBM cell growth, further increasing its channel activity is not sufficient to promote malignancy in the tested cell culture condition. To identify *PIEZO1* target genes

Figure 4. Human *PIEZO1* Expression Correlates with Glioma Aggressiveness and Regulates GBM Growth

- (A) Heatmap of 345 *PIEZO1*-correlated genes in TCGA LGG-GBM RNA-seq dataset ($n = 702$). Based on hierarchical clustering, patient tumors are sub-classified into *PIEZO1* high, *PIEZO1* moderate, and *PIEZO1* low groups. The gliomas are annotated by WHO neoplasm grade, TCGA histological class, histological class plus WHO grades, astrocytoma component, IDH mutation, 1p/19q co-deletion, G-CIMP phenotype, MGMT promoter methylation, DNA methylation clusters, and molecular subtypes.
- (B) Kaplan-Meier survival analysis shows that patients with high *PIEZO1* expression in TCGA LGG and LGG-GBM datasets show worse overall survival.
- (C) Representative whole-cell recording traces of mechanically activated currents recorded in response to stimulation by hypertonic or isotonic solutions puffed at either soma or cellular process at holding potential of -80 mV from the G532 GBM stem cell (schematic illustration). Quantifications are shown for current fold differences at 100 mmHg, as well as mechanosensitive current in cells treated with scrambled shRNA and *PIEZO1* shRNA. Error bars, mean \pm SEM.
- (D) *PIEZO1* knockdown suppresses the clonogenic growth of human GBM cell lines (GS2, SF7225, and SF7881). Representative images for three biological replicates are shown.
- (E) *PIEZO1* knockdown decreases the proliferation of human GBM stem cell lines (G508 and G532). Error bars, mean \pm SEM.
- (F) *PIEZO1* knockdown reduces the sphere formation capacity of human GBM stem cell lines (G508 and G532). Error bars, mean \pm SEM.
- (G) Bioluminescence imaging shows that doxycycline-dependent inducible *PIEZO1* knockdown after tumor implantation inhibits the growth of G411 xenograft GBM *in vivo*.
- (H) Kaplan-Meier survival analysis of mice bearing G532 and G411 xenograft tumors with constitutive *PIEZO1* knockdown compared to control, and mice bearing G411 xenograft tumors with inducible *PIEZO1* knockdown compared to control.



(legend on next page)

with high confidence, we performed RNA sequencing of two GBM stem cell lines (G508 and G532) with and without PIEZO1 knockdown and found that multiple pathways, such as those in mitotic cell cycle, focal adhesion, ECM, and response to mechanical stimulus, were altered (Figures 6G and S9). We performed computational analysis to identify the common genes detected both as *PIEZO1*-correlated genes from TCGA datasets and altered genes after *PIEZO1* knockdown from these two GBM stem cell lines. Strikingly, this unbiased, large-scale bioinformatics interrogation of both human tumor datasets and differential gene expression after *PIEZO1* knockdown in glioma cells revealed a total of nine genes as high-confidence *PIEZO1* target genes (Figure 6H). Among them, four genes (*PLOD1*, *MMP14*, *ADAM9*, and *PLAU*) are known to control ECM remodeling, *FHL3* controls actin cytoskeleton, and *TAZ* regulates the mechanosensitive HIPPO signaling pathway (Figure 6I). Taken together, these data suggest that *PIEZO1* not only relays mechanical input to promote glioma growth, but also actively modulates ECM and other mechanotransduction mechanisms in the tumor.

DISCUSSION

The interplay between physical forces and biochemical signaling pathways controls tumor initiation and progression. Although the impact of force on tumor malignancy was described several decades ago, the molecules that detect mechanical input and transduce physical force into intracellular signaling have yet to be fully identified. While *PIEZO* channel-mediated mechanotransduction is critical for many physiological sensory functions such as touch and proprioception, we report here a previously unrecognized *in vivo* role of *PIEZO* to promote tumor aggression by increasing tissue stiffening, a physical feature of solid tumors. Mouse *Piezo1* and human *PIEZO1* can rescue the glioma growth defect caused by genetic knockout of endogenous *Drosophila Piezo*, highlighting that the *PIEZO* class of mechanosensitive ion channels has evolutionarily conserved function in tumors. The fact that *Drosophila Piezo* regulates gliomas driven by highly distinct oncogenic mutations and signaling pathways, and that *PIEZO1* is overexpressed across multiple types of human solid tumors, suggests that *PIEZO*-mediated mechanosensation and

signaling may serve as a general mechanism for tumors to perceive and respond to their aberrant tissue mechanics. Tumor tissue stiffening provides a mechanical microenvironment to activate *PIEZO1*, the activity of which promotes the assembly of focal adhesions and activates integrin-FAK signaling. *PIEZO1* signaling regulates proliferation and the expression of genes involved in ECM remodeling, which can further modulate tissue stiffness. In turn, the stiffer environment upregulates *PIEZO1* expression to increase the mechanosensory and mechanotransduction capacity of the tumor cells. Therefore, glioma cells are mechanosensory and these processes form a reciprocal, disease-aggravating feedforward circuit between *PIEZO1*-dependent mechanotransduction and aberrant tissue mechanics in gliomas (Figure 7). A dual role for *PIEZO1* has been reported in regulating tissue homeostasis. *PIEZO1* promotes live-cell extrusion in overcrowded epithelial tissue, providing a potential tumor-suppressive mechanism (Eisenhoffer et al., 2012). *PIEZO1* activity also stimulates a proliferative response to increase cell density when tissue stretching or wounding results in a sparse cell distribution (Gudipaty et al., 2017). Our findings demonstrate that this cell contact-dependent, balanced *PIEZO1* function is lost upon tumorigenesis, and oncogenically transformed cells, which resist contact inhibition and densely populate the tumor tissue, rewire the mechanosensory function of *PIEZO1* to unidirectionally promote malignant progression.

Our bioinformatics study identified that *PIEZO1* promoter is generally hyper-methylated in the IDH mutant gliomas, and this correlates with decreased *PIEZO1* mRNA expression in these tumors. This finding suggests that the generally more aggressive IDH wild-type gliomas are epigenetically more poised to overexpress *PIEZO1*. Whether various growth factor signaling pathways that are active in the IDH wild-type glioma subtypes further upregulate *PIEZO1* expression is an interesting topic that warrants future investigation. Since aggressive gliomas markedly overexpress *PIEZO1*, tumor-specific pharmacological inhibition of *PIEZO1* may demonstrate therapeutic efficacy. Currently identified inhibitors, such as ruthenium red, Gd^{3+} , or the spider peptide toxin GsMTx4, are not *PIEZO1* specific and act on a variety of ion channels that have mechanosensitive properties. Recent high-throughput screenings identified three small

Figure 5. *PIEZO1* Localizes at Focal Adhesion to Promote Its Assembly and Activate Integrin-Focal Adhesion Kinase Signaling

(A) Core pathway mapping of gene networks that are positively correlated with *PIEZO1* expression in the TCGA LGG-GBM dataset. GO biological processes, GO cellular components, GO molecular functions, and KEGG pathways that associated with tumor stiffness and tumorigenesis are enriched. Genes and pathways positively correlated with *PIEZO1* expression are colored yellow and red, respectively.

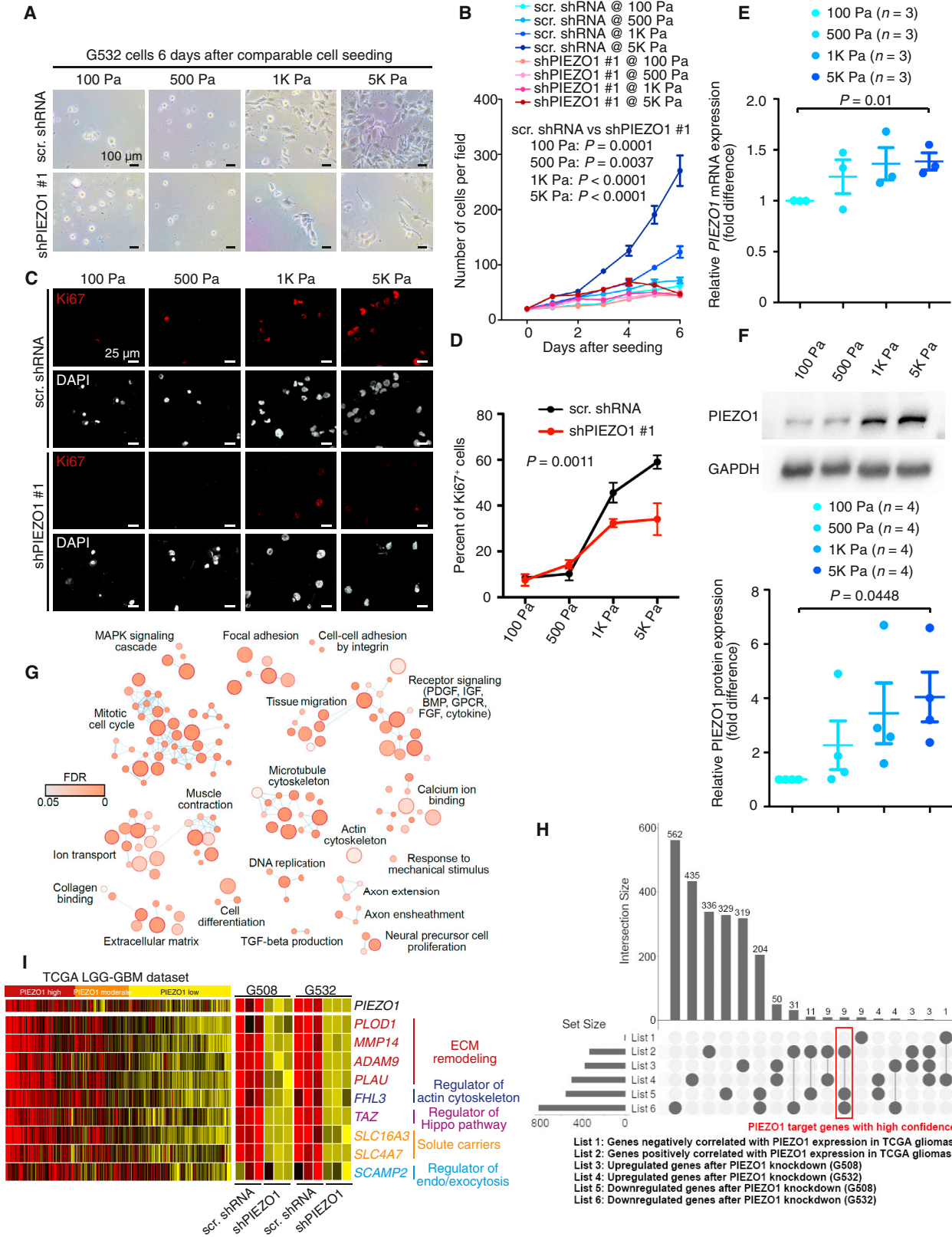
(B) Heatmap of *PIEZO1*-correlated genes enriched in multiple pathways that regulate tissue stiffness and tumorigenesis. Genes are annotated with enriched pathways. Row annotation (Pathway IDs): 1, GO MF Integrin binding; 2, GO MF Actin filament binding; 3, KEGG PI3K-Akt signaling pathway; 4, KEGG Pathways in cancer; 5, KEGG Focal adhesion; 6, KEGG ECM-receptor interaction; 7, GO CC Focal adhesion; 8, GO CC Extracellular matrix; 9, GO CC Actin cytoskeleton; 10, GO BP Cellular response to mechanical stimulus; 11, GO BP extracellular matrix organization; 12, GO BP Collagen catabolic process; 13, GO BP Cell adhesion.

(C) Immunocytochemical co-staining of *PIEZO1* and activated $\beta 1$ integrin, Vinculin, Paxillin, or FAK in the G532 GBM stem cells. Representative images for three biological replicates are shown.

(D) Immunocytochemical staining of *PIEZO1*, activated $\beta 1$ integrin, Vinculin, FAK, or phosphorylated Paxillin with or without *PIEZO1* knockdown in the G532 GBM stem cells. Representative images for three biological replicates are shown.

(E) Quantifications of the effect of *PIEZO1* knockdown on focal adhesions and integrin-FAK signaling. Data are from three biological replicates. Data point numbers for scrambled shRNA and sh*PIEZO1* #1: 26 and 28 for *PIEZO1* puncta size, 26 and 28 for *PIEZO1* intensity, 17 and 18 for $\beta 1$ integrin^{ACT} size, 17 and 18 for $\beta 1$ integrin^{ACT} intensity, 23 and 24 for Vinculin size, 23 and 24 for Vinculin intensity, 18 and 22 for FAK size, 18 and 22 for FAK intensity, 15 and 20 for Phospho-Paxillin (Tyr118) size, 15 and 20 for Phospho-Paxillin (Tyr118) intensity, respectively. Error bars, mean \pm SEM.

(F) Immunoblotting and quantifications of *PIEZO1*, FAK, and pFAK in G532 cells treated with two different *PIEZO1* shRNA compared to control. Error bars, mean \pm SEM.



(legend on next page)

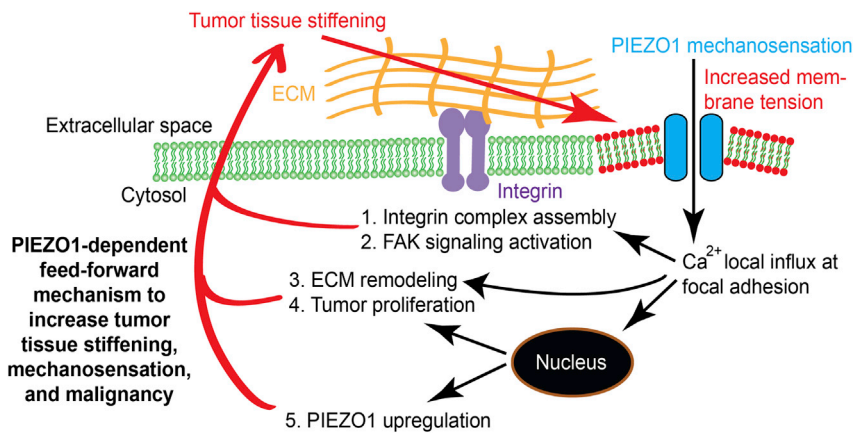


Figure 7. A Proposed Model Showing the Reciprocal, Disease-Agravating, PIEZO1-Dependent Feedforward Circuit between Tumor Cell Mechanotransduction and Aberrant Tissue Mechanics in Gliomas

During disease progression, tumor tissue stiffening provides a favored mechanical microenvironment to activate PIEZO1, which localizes at various tumor cell regions including focal adhesion. PIEZO1 regulates the assembly of focal adhesions, activation of integrin-focal adhesion signaling, tumor cell proliferation, and the expression of a number of genes involved in ECM remodeling. In addition, tissue stiffening in the tumor further increases the mRNA and protein level of PIEZO1, which in turn elevates the mechanosensory and mechanotransduction capacity of the tumor cells. These processes form a reciprocal, feedforward circuit between tumor cell mechanotransduction and aberrant tissue mechanics in gliomas to promote malignancy.

molecule chemical activators of PIEZO1, Yoda1, Jedi1, and Jedi2 (Syeda et al., 2015; Wang et al., 2018), which affect PIEZO1 channel activity by regulating its sensitivity or inactivation kinetics of mechanically induced responses, suggesting that PIEZO1 is amenable to pharmacological modulations. Interestingly, these compounds display no discernible impact on PIEZO2. As high-resolution structure of PIEZO1 recently became available (Saotome et al., 2018; Zhao et al., 2018), rationally designed compound screening should facilitate the development of highly specific pharmacological modulators of PIEZO1 as novel therapeutics. PIEZO1 and PIEZO2 are expressed in different organs and each in general regulates a distinct set of physiological functions. For example, PIEZO1 controls vascular homeostasis (Li et al., 2014; Ranade et al., 2014a), blood pressure (Wang et al., 2016), and axon growth (Koser et al., 2016), while PIEZO2 functions in mediating touch (Ranade et al., 2014b), proprioception (Woo et al., 2015), airway stretch, and lung inflation (Nonomura et al., 2017). Although we found that *PIEZO2* expression is not prognostic in glioma, PIEZO2 was recently shown to regulate breast cancer cell migration *in vitro* (Pardo-Pastor et al., 2018). Future experiments using animal models to examine the *in vivo* function of PIEZO2 and

assess the therapeutic potential to target PIEZO2 in cancer are warranted.

Brain tumors, like many other types of solid tumors, display considerable levels of genetic and cellular heterogeneity. For example, brain tumors can be categorized into distinct subtypes based on mutational signatures and major signaling pathways that regulate tumor initiation, maintenance, or progression (Cavalli et al., 2017; Huse et al., 2013; Verhaak et al., 2010). It is striking that high *PIEZO1* expression is not associated with a specific glioma subtype, and its overexpression is found in LGGs or HGGs with worse prognosis caused by a variety of genetic alterations. We suggest that this association between *PIEZO1* expression and the aggressive glioma phenotype is consistent with the increasing tissue stiffening as tumorigenesis proceeds, and PIEZO1 upregulation and function amplify the level and speed of tissue stiffening to aggravate disease progression. PIEZO1 function in glioma may be conserved in other types of human cancers that overexpress PIEZO1, and our findings may stimulate evaluation of the potential to target other types of mechanosensitive ion channels in cancer. In addition to genetic heterogeneity, brain tumors consist of a hierarchy of cell types. Situated at the apex of tumor cellular hierarchy, brain

Figure 6. A Reciprocal PIEZO1-Dependent Feedforward Mechanism Regulates Glioma Tissue Mechanics and Tumor Malignancy

- (A) Representatively areas of comparably plated G532 GBM stem cells display stiffness-dependent growth increase, a process that is abrogated by PIEZO1 knockdown.
- (B) Quantifications of the number of the control and PIEZO1-deficient GBM stem cells cultured at various levels of stiffness. Cell numbers were quantified in five randomly selected imaging fields in three biological replicates. Error bars, mean \pm SEM.
- (C) Immunocytochemical staining of Ki67 of G532 GBM stem cells cultured at various levels of stiffness, treated with scrambled shRNA or PIEZO1 shRNA. Cell nuclei were stained by DAPI.
- (D) Quantifications of the percentage of Ki67⁺ actively cycling control and PIEZO1-deficient GBM stem cells cultured at various levels of stiffness. Cells were quantified in five randomly selected imaging fields in three biological replicates. Error bars, mean \pm SEM.
- (E) *PIEZO1* mRNA levels of G532 GBM stem cells cultured at various levels of stiffness. Error bars, mean \pm SEM.
- (F) *PIEZO1* protein levels of G532 GBM stem cells cultured at various levels of stiffness. Error bars, mean \pm SEM.
- (G) RNA-seq of two GBM stem cell lines (G508 and G532) with and without PIEZO1 knockdown shows that multiple pathways, including those regulating mitotic cell cycle, focal adhesion, actin cytoskeleton, cell-cell adhesion, ECM, and response to mechanical stimulus, are altered.
- (H) UpSet plot identifies common genes detected both as *PIEZO1*-correlated genes based on TCGA datasets and altered genes after PIEZO1 knockdown in G508 and G532 stem cell lines. Nine genes are identified as high-confidence PIEZO1 target genes.
- (I) Heatmap shows expression of the nine high-confidence PIEZO1 target genes in TCGA LGG-GBM dataset and GBM cells. Note that four out of the nine genes control ECM remodeling, one gene regulates actin cytoskeleton, and one gene regulates the mechanosensitive HIPPO signaling pathway.

tumor-initiating cells (BTICs) are rare tumor cells that give rise to both transiently proliferative and differentiated tumor cells. BTICs resist conventional anti-mitotic therapy that targets only rapidly dividing cells; hence, they are the root for tumor initiation and recurrence. It would be of both scientific and clinical significance to determine whether various tumor cell types display different dependencies on physical cues provided by their microenvironment, and define tumor cell-type-specific mechanosensation and mechanotransduction mechanisms.

STAR★METHODS

Detailed methods are provided in the online version of this paper and include the following:

- **KEY RESOURCES TABLE**
- **CONTACT FOR REAGENT AND RESOURCE SHARING**
- **EXPERIMENTAL MODEL AND SUBJECT DETAILS**
 - *Drosophila* stocks
 - *Drosophila* study
 - Patient samples and cell culture
 - Mice
- **METHOD DETAILS**
 - *Drosophila* immunostaining, confocal microscopy and image quantifications
 - Generating cell culture coverslips with various levels of stiffness, cell counting, self-renewal assay and immunofluorescence staining
 - Patient tissue staining and Microscopy
 - Real-Time Quantitative PCR
 - Lentivirus-mediated shRNA study
 - Xenograft and *in vivo* bioluminescence imaging
 - Bioinformatics study
 - *PIEZO1* promoter methylation analysis
 - Atomic force microscopy
 - Western blotting
 - Generation of *PIEZO1* deficient HEK293T clones
 - Electrophysiology
- **QUANTIFICATION AND STATISTICAL ANALYSIS**
- **DATA AND SOFTWARE AVAILABILITY**

SUPPLEMENTAL INFORMATION

Supplemental Information includes nine figures and one table and can be found with this article online at <https://doi.org/10.1016/j.neuron.2018.09.046>.

A video abstract is available at <https://doi.org/10.1016/j.neuron.2018.09.046#mmc3>.

ACKNOWLEDGMENTS

This work is supported by SickKids Foundation, Arthur and Sonia Labatt Brain Tumour Research Centre, Garron Family Cancer Centre, b.r.a.i.n.child, Meagan's Walk, Natural Sciences and Engineering Research Council (NSERC) Discovery Grant, and Ontario Institute for Cancer Research (OICR) Translational Research Initiative (BC-TRI-FR-HSK) to X.H., and Canadian Institutes of Health Research (CIHR) Project Grants to X.H., L.-Y.W. (PJT 156439), and C.-c.H. We thank Krzysztof Jagla, Marta Llimargas, and Dorothea Godt for fly stocks. We thank Michael Taylor for constructive suggestions on the project and his lab for technical support. We thank Samantha Stehbens for technical advice on studying focal adhesions. We are grateful for Paul Paroutis and Kimberly Lau at the SickKids Imaging Facility for their help on confocal imaging

and image analysis. We thank Shan Meltzer and all Huang lab members for critical reading of the manuscript, and Zexin Chen for helping with drawing the schematic in Figure 1C. X.H. thanks the love and support from Lucas Huang and Liam Huang. X.H. is a Catalyst Scholar at The Hospital for Sick Children and Canada Research Chair in Cancer Biophysics.

AUTHOR CONTRIBUTIONS

Conception of project, X.H. Experimental design, data acquisition, and interpretation, X.C., S.W., A.B., M.Z., W. Dong, J.J.F., H.-K.M., W.C.Y., M.H., D.D., W. Dou, F.L., F.J.C., H.W., M.M.K., P.B.D., Y. Song, C.-c.H., Y. Sun, L.-Y.W., X.L., and X.H. Manuscript writing, X.C. and X.H.

DECLARATION OF INTERESTS

The authors declare no competing financial interests.

Received: May 2, 2018

Revised: August 31, 2018

Accepted: September 25, 2018

Published: October 18, 2018

SUPPORTING CITATIONS

The following references appear in the Supplemental Information: Bataillé et al. (2010); Beumer et al. (1999); Martin-Bermudo et al. (1997); Moussian et al. (2015); Tsai et al. (2012).

REFERENCES

- Agnihotri, S., Burrell, K.E., Wolf, A., Jalali, S., Hawkins, C., Rutka, J.T., and Zadeh, G. (2013). Glioblastoma, a brief review of history, molecular genetics, animal models and novel therapeutic strategies. *Arch. Immunol. Ther. Exp. (Warsz.)* 61, 25–41.
- Aguilar-Cuenca, R., Juanes-García, A., and Vicente-Manzanares, M. (2014). Myosin II in mechanotransduction: master and commander of cell migration, morphogenesis, and cancer. *Cell. Mol. Life Sci.* 71, 479–492.
- Bataillé, L., Delon, I., Da Ponte, J.P., Brown, N.H., and Jagla, K. (2010). Downstream of identity genes: muscle-type-specific regulation of the fusion process. *Dev. Cell* 19, 317–328.
- Beumer, K.J., Rohrbough, J., Prokop, A., and Broadie, K. (1999). A role for PS integrins in morphological growth and synaptic function at the postembryonic neuromuscular junction of *Drosophila*. *Development* 126, 5833–5846.
- Cavalli, F.M.G., Remke, M., Rampasek, L., Peacock, J., Shih, D.J.H., Luu, B., Garzia, L., Torchia, J., Nor, C., Morrissy, A.S., et al. (2017). Intertumoral heterogeneity within medulloblastoma subgroups. *Cancer Cell* 31, 737–754.e6.
- Chesler, A.T., Szczot, M., Bharucha-Goebel, D., Čeko, M., Donkervoort, S., Laubacher, C., Hayes, L.H., Alter, K., Zampieri, C., Stanley, C., et al. (2016). The role of *PIEZO2* in human mechanosensation. *N. Engl. J. Med.* 375, 1355–1364.
- Coste, B., Murthy, S.E., Mathur, J., Schmidt, M., Mechoukhi, Y., Delmas, P., and Patapoutian, A. (2015). *Piezo1* ion channel pore properties are dictated by C-terminal region. *Nat. Commun.* 6, 7223.
- Cox, C.D., Bae, C., Ziegler, L., Hartley, S., Nikolova-Krstevski, V., Rohde, P.R., Ng, C.A., Sachs, F., Gottlieb, P.A., and Martinac, B. (2016). Removal of the mechanoprotective influence of the cytoskeleton reveals *PIEZO1* is gated by bilayer tension. *Nat. Commun.* 7, 10366.
- Eisenhoffer, G.T., Loftus, P.D., Yoshigi, M., Otsuna, H., Chien, C.B., Morcos, P.A., and Rosenblatt, J. (2012). Crowding induces live cell extrusion to maintain homeostatic cell numbers in epithelia. *Nature* 484, 546–549.
- Frattini, V., Pagnotta, S.M., Tala, Fan, J.J., Russo, M.V., Lee, S.B., Garofano, L., Zhang, J., Shi, P., Lewis, G., et al. (2018). A metabolic function of *FGFR3-TACC3* gene fusions in cancer. *Nature* 553, 222–227.

- Ge, J., Li, W., Zhao, Q., Li, N., Chen, M., Zhi, P., Li, R., Gao, N., Xiao, B., and Yang, M. (2015). Architecture of the mammalian mechanosensitive Piezo1 channel. *Nature* 527, 64–69.
- Gudipaty, S.A., Lindblom, J., Loftus, P.D., Redd, M.J., Edes, K., Davey, C.F., Krishnegowda, V., and Rosenblatt, J. (2017). Mechanical stretch triggers rapid epithelial cell division through Piezo1. *Nature* 543, 118–121.
- He, L., Si, G., Huang, J., Samuel, A.D.T., and Perrimon, N. (2018). Mechanical regulation of stem-cell differentiation by the stretch-activated Piezo channel. *Nature* 555, 103–106.
- Huse, J.T., Holland, E., and DeAngelis, L.M. (2013). Glioblastoma: molecular analysis and clinical implications. *Annu. Rev. Med.* 64, 59–70.
- Jia, Z., Ikeda, R., Ling, J., Viatchenko-Karpinski, V., and Gu, J.G. (2016). Regulation of Piezo2 mechanotransduction by static plasma membrane tension in primary afferent neurons. *J. Biol. Chem.* 291, 9087–9104.
- Kai, F., Laklai, H., and Weaver, V.M. (2016). Force matters: biomechanical regulation of cell invasion and migration in disease. *Trends Cell Biol.* 26, 486–497.
- Kim, C., Ye, F., and Ginsberg, M.H. (2011). Regulation of integrin activation. *Annu. Rev. Cell Dev. Biol.* 27, 321–345.
- Kim, S.E., Coste, B., Chadha, A., Cook, B., and Patapoutian, A. (2012). The role of *Drosophila* Piezo in mechanical nociception. *Nature* 483, 209–212.
- Koser, D.E., Thompson, A.J., Foster, S.K., Dwivedy, A., Pillai, E.K., Sheridan, G.K., Svoboda, H., Viana, M., Costa, L.D., Guck, J., et al. (2016). Mechanosensing is critical for axon growth in the developing brain. *Nat. Neurosci.* 19, 1592–1598.
- Lewis, A.H., and Grandl, J. (2015). Mechanical sensitivity of Piezo1 ion channels can be tuned by cellular membrane tension. *eLife* 4, e12088.
- Li, J., Hou, B., Tumova, S., Muraki, K., Bruns, A., Ludlow, M.J., Sedo, A., Hyman, A.J., McKeown, L., Young, R.S., et al. (2014). Piezo1 integration of vascular architecture with physiological force. *Nature* 515, 279–282.
- Li, C., Rezaia, S., Kammerer, S., Sokolowski, A., Devaney, T., Gorischek, A., Jahn, S., Hackl, H., Groschner, K., Windpassinger, C., et al. (2015). Piezo1 forms mechanosensitive ion channels in the human MCF-7 breast cancer cell line. *Sci. Rep.* 5, 8364.
- Martin-Bermudo, M.D., Dunin-Borkowski, O.M., and Brown, N.H. (1997). Specificity of PS integrin function during embryogenesis resides in the alpha subunit extracellular domain. *EMBO J.* 16, 4184–4193.
- Martins, J.R., Penton, D., Peyronnet, R., Arhatte, M., Moro, C., Picard, N., Kurt, B., Patel, A., Honoré, E., and Demolombe, S. (2016). Piezo1-dependent regulation of urinary osmolarity. *Pflugers Arch.* 468, 1197–1206.
- Miroshnikova, Y.A., Mouw, J.K., Barnes, J.M., Pickup, M.W., Lakins, J.N., Kim, Y., Lobo, K., Persson, A.I., Reis, G.F., McKnight, T.R., et al. (2016). Tissue mechanics promote IDH1-dependent HIF1 α -tenascin C feedback to regulate glioblastoma aggression. *Nat. Cell Biol.* 18, 1336–1345.
- Moussian, B., Letizia, A., Martínez-Corrales, G., Rotstein, B., Casali, A., and Llimargas, M. (2015). Deciphering the genetic programme triggering timely and spatially-regulated chitin deposition. *PLoS Genet.* 11, e1004939.
- Murthy, S.E., Dubin, A.E., and Patapoutian, A. (2017). Piezos thrive under pressure: mechanically activated ion channels in health and disease. *Nat. Rev. Mol. Cell Biol.* 18, 771–783.
- Nonomura, K., Woo, S.H., Chang, R.B., Gillich, A., Qiu, Z., Francisco, A.G., Ranade, S.S., Liberles, S.D., and Patapoutian, A. (2017). Piezo2 senses airway stretch and mediates lung inflation-induced apnoea. *Nature* 541, 176–181.
- Northey, J.J., Przybyla, L., and Weaver, V.M. (2017). Tissue force programs cell fate and tumor aggression. *Cancer Discov.* 7, 1224–1237.
- Oudin, M.J., and Weaver, V.M. (2016). Physical and chemical gradients in the tumor microenvironment regulate tumor cell invasion, migration, and metastasis. *Cold Spring Harb. Symp. Quant. Biol.* 81, 189–205.
- Pajic, M., Herrmann, D., Vennin, C., Conway, J.R., Chin, V.T., Johnsson, A.K., Welch, H.C., and Timpson, P. (2015). The dynamics of Rho GTPase signaling and implications for targeting cancer and the tumor microenvironment. *Small GTPases* 6, 123–133.
- Pardo-Pastor, C., Rubio-Moscardo, F., Vogel-González, M., Serra, S.A., Afthinos, A., Mrkonjic, S., Destaing, O., Abenza, J.F., Fernández-Fernández, J.M., Trepát, X., et al. (2018). Piezo2 channel regulates RhoA and actin cytoskeleton to promote cell mechanobiological responses. *Proc. Natl. Acad. Sci. USA* 115, 1925–1930.
- Parker, B.C., Annala, M.J., Cogdell, D.E., Granberg, K.J., Sun, Y., Ji, P., Li, X., Gumin, J., Zheng, H., Hu, L., et al. (2013). The tumorigenic FGFR3-TACC3 gene fusion escapes miR-99a regulation in glioblastoma. *J. Clin. Invest.* 123, 855–865.
- Penman, C.L., Faulkner, C., Lowis, S.P., and Kurian, K.M. (2015). Current understanding of BRAF alterations in diagnosis, prognosis, and therapeutic targeting in pediatric low-grade gliomas. *Front. Oncol.* 5, 54.
- Pollard, S.M., Yoshikawa, K., Clarke, I.D., Danovi, D., Stricker, S., Russell, R., Bayani, J., Head, R., Lee, M., Bernstein, M., et al. (2009). Glioma stem cell lines expanded in adherent culture have tumor-specific phenotypes and are suitable for chemical and genetic screens. *Cell Stem Cell* 4, 568–580.
- Przybyla, L., Muncie, J.M., and Weaver, V.M. (2016). Mechanical control of epithelial-to-mesenchymal transitions in development and cancer. *Annu. Rev. Cell Dev. Biol.* 32, 527–554.
- Ranade, S.S., Qiu, Z., Woo, S.H., Hur, S.S., Murthy, S.E., Cahalan, S.M., Xu, J., Mathur, J., Bandell, M., Coste, B., et al. (2014a). Piezo1, a mechanically activated ion channel, is required for vascular development in mice. *Proc. Natl. Acad. Sci. USA* 111, 10347–10352.
- Ranade, S.S., Woo, S.H., Dubin, A.E., Moshourab, R.A., Wetzel, C., Petrus, M., Mathur, J., Bégay, V., Coste, B., Mainquist, J., et al. (2014b). Piezo2 is the major transducer of mechanical forces for touch sensation in mice. *Nature* 516, 121–125.
- Rape, A.D., and Kumar, S. (2014). A composite hydrogel platform for the dissection of tumor cell migration at tissue interfaces. *Biomaterials* 35, 8846–8853.
- Rape, A.D., Zibinsky, M., Murthy, N., and Kumar, S. (2015). A synthetic hydrogel for the high-throughput study of cell-ECM interactions. *Nat. Commun.* 6, 8129.
- Read, R.D., Cavenee, W.K., Furnari, F.B., and Thomas, J.B. (2009). A *drosophila* model for EGFR-Ras and PI3K-dependent human glioma. *PLoS Genet.* 5, e1000374.
- Rode, B., Shi, J., Endesh, N., Drinkhill, M.J., Webster, P.J., Lotteau, S.J., Bailey, M.A., Yuldasheva, N.Y., Ludlow, M.J., Cubbon, R.M., et al. (2017). Piezo1 channels sense whole body physical activity to reset cardiovascular homeostasis and enhance performance. *Nat. Commun.* 8, 350.
- Saotome, K., Murthy, S.E., Kefauver, J.M., Whitwam, T., Patapoutian, A., and Ward, A.B. (2018). Structure of the mechanically activated ion channel Piezo1. *Nature* 554, 481–486.
- Seo, B.R., Bhardwaj, P., Choi, S., Gonzalez, J., Andresen Eguiluz, R.C., Wang, K., Mohanan, S., Morris, P.G., Du, B., Zhou, X.K., et al. (2015). Obesity-dependent changes in interstitial ECM mechanics promote breast tumorigenesis. *Sci. Transl. Med.* 7, 301ra130.
- Singh, D., Chan, J.M., Zoppoli, P., Niola, F., Sullivan, R., Castano, A., Liu, E.M., Reichel, J., Porrati, P., Pellegatta, S., et al. (2012). Transforming fusions of FGFR and TACC genes in human glioblastoma. *Science* 337, 1231–1235.
- Syeda, R., Xu, J., Dubin, A.E., Coste, B., Mathur, J., Huynh, T., Matzen, J., Lao, J., Tully, D.C., Engels, I.H., et al. (2015). Chemical activation of the mechanotransduction channel Piezo1. *eLife* 4, <https://doi.org/10.7554/eLife.07369>.
- Syeda, R., Florendo, M.N., Cox, C.D., Kefauver, J.M., Santos, J.S., Martinac, B., and Patapoutian, A. (2016). Piezo1 channels are inherently mechanosensitive. *Cell Rep.* 17, 1739–1746.
- Tsai, P.I., Wang, M., Kao, H.H., Cheng, Y.J., Lin, Y.J., Chen, R.H., and Chien, C.T. (2012). Activity-dependent retrograde laminin A signaling regulates synapse growth at *Drosophila* neuromuscular junctions. *Proc. Natl. Acad. Sci. USA* 109, 17699–17704.

- Tung, J.C., Barnes, J.M., Desai, S.R., Sistrunk, C., Conklin, M.W., Schedin, P., Eliceiri, K.W., Keely, P.J., Seewaldt, V.L., and Weaver, V.M. (2015). Tumor mechanics and metabolic dysfunction. *Free Radic. Biol. Med.* *79*, 269–280.
- Umesh, V., Rape, A.D., Ulrich, T.A., and Kumar, S. (2014). Microenvironmental stiffness enhances glioma cell proliferation by stimulating epidermal growth factor receptor signaling. *PLoS ONE* *9*, e101771.
- Verhaak, R.G., Hoadley, K.A., Purdom, E., Wang, V., Qi, Y., Wilkerson, M.D., Miller, C.R., Ding, L., Golub, T., Mesirov, J.P., et al.; Cancer Genome Atlas Research Network (2010). Integrated genomic analysis identifies clinically relevant subtypes of glioblastoma characterized by abnormalities in PDGFRA, IDH1, EGFR, and NF1. *Cancer Cell* *17*, 98–110.
- Volkers, L., Mechioukhi, Y., and Coste, B. (2015). Piezo channels: from structure to function. *Pflügers Arch.* *467*, 95–99.
- Wang, S., Chennupati, R., Kaur, H., Iring, A., Wettschureck, N., and Offermanns, S. (2016). Endothelial cation channel PIEZO1 controls blood pressure by mediating flow-induced ATP release. *J. Clin. Invest.* *126*, 4527–4536.
- Wang, Y., Chi, S., Guo, H., Li, G., Wang, L., Zhao, Q., Rao, Y., Zu, L., He, W., and Xiao, B. (2018). A lever-like transduction pathway for long-distance chemical- and mechano-gating of the mechanosensitive Piezo1 channel. *Nat. Commun.* *9*, 1300.
- Woo, S.H., Lukacs, V., de Nooij, J.C., Zaytseva, D., Criddle, C.R., Francisco, A., Jessell, T.M., Wilkinson, K.A., and Patapoutian, A. (2015). Piezo2 is the principal mechanotransduction channel for proprioception. *Nat. Neurosci.* *18*, 1756–1762.
- Wu, J., Lewis, A.H., and Grandl, J. (2017). Touch, tension, and transduction - the function and regulation of Piezo ion channels. *Trends Biochem. Sci.* *42*, 57–71.
- Yu, F.X., and Guan, K.L. (2013). The Hippo pathway: regulators and regulations. *Genes Dev.* *27*, 355–371.
- Zhao, Q., Zhou, H., Chi, S., Wang, Y., Wang, J., Geng, J., Wu, K., Liu, W., Zhang, T., Dong, M.Q., et al. (2018). Structure and mechanogating mechanism of the Piezo1 channel. *Nature* *554*, 487–492.

STAR★METHODS

KEY RESOURCES TABLE

| REAGENT or RESOURCE | SOURCE | IDENTIFIER |
|---|---|----------------------------------|
| Antibodies | | |
| mouse anti-Repo antibody | DSHB | Cat#8D12; RRID: AB_528448 |
| rabbit anti-Histone H3 (phospho S10) antibody | ABCAM | Cat#ab5176; RRID: AB_304763 |
| Alexa Fluor 488 Phalloidin | Thermo Fisher Scientific | Cat#A12379; RRID: AB_2315147 |
| rabbit anti-phosphorylated FAK (Tyr397)antibody | Thermo Fisher Scientific | Cat#44-624G; RRID: AB_2533701 |
| rabbit anti-PIEZO1 antibody | Proteintech | Cat#15939-1-AP; RRID: AB_2231460 |
| mouse anti-Integrin beta 1 antibody [12G10] | ABCAM | Cat#ab30394; RRID: AB_775726 |
| mouse anti-Vinculin antibody | EMD Millipore | Cat#MAB3574; RRID: AB_2304338 |
| mouse anti-FAK antibody | BD Biosciences | Cat#610088; RRID: AB_397495 |
| mouse anti-Paxillin antibody | BD Biosciences | Cat#610051; RRID: AB_397463 |
| rabbit anti-phosphorylated Paxillin (Tyr118) antibody | Invitrogen | Cat#44-722G; RRID: AB_2533733 |
| rabbit anti-Ki67 antibody | ABCAM | Cat#ab15580; RRID: AB_443209 |
| mouse anti-alpha Tubulin | Sigma Aldrich | Cat#T6199; RRID: AB_477583 |
| rabbit anti-GAPDH | New England Biolabs | Cat#2118S; RRID: AB_561053 |
| Bacterial and Virus Strains | | |
| plasmid: pBMN (CMV-copGFP-Luc2-Puro) | Addgene | Plasmid #80389 |
| Plasmid: pLKO.1-shPIEZO1 #1 | Dharmacon | Clone ID: TRCN0000121969 |
| plasmid: pLKO.1-shPIEZO1 #2 | Dharmacon | Clone ID: TRCN0000142459 |
| plasmid: pTRIPZ-Tet-ON-shPEIZO1 #1 | Dharmacon | Clone ID: V3THS_361173 |
| plasmid: pTRIPZ-Tet-ON-shPEIZO1 #2 | Dharmacon | Clone ID: V3THS_361177 |
| Biological Samples | | |
| Primary GBM samples | University of Toronto Brain Tumor Bank; St. Michael's Hospital/Toronto Western Hospital | N/A |
| Chemicals, Peptides, and Recombinant Proteins | | |
| XenoLight D-Luciferin Potassium Salt | PerkinElmer Health Sciences Canada | Cat#122799 |
| Sulfo SANPAH Crosslinker | Sigma Aldrich | Cat#803332 |
| Poly-L-ornithine solution | Sigma Aldrich | Cat#P4957 |
| Laminin from Engelbreth-Holm-Swarm murine sarcoma basement membrane | Sigma Aldrich | Cat#L2020 |
| Yoda1 | TOCRIS | Cat#5586 |
| NeuroCult NS-A Basal Medium (Human) | StemCell Technologies | Cat#05750 |
| Recombinant human EGF | Sigma Aldrich | Cat#E9644 |
| Basic FGF | StemCell Technologies | Cat#02634 |
| Puromycin dihydrochloride from Streptomyces alboniger | Sigma Aldrich | Cat#P8833 |
| Doxycycline hyclate | Sigma Aldrich | Cat#D9891 |
| Rodent Diet (2018, 625 Doxycycline) | Envigo | Diet#TD.120769 |
| Critical Commercial Assays | | |
| Trypan Blue Solution, 0.4% | Thermo Fisher Scientific | Cat#15250061 |
| ImmPress HRP Anti-Rabbit IgG (Peroxidase) | Vector Laboratories | Cat#MP-7401 |
| Polymer Detection Kit,made in Horse | | |
| PureLink™ RNA mini kit | Thermo Fisher Scientific | Cat#12183018A |
| Deposited Data | | |
| Raw and analyzed RNA-seq data | This paper | GEO: GSE113261 |

(Continued on next page)

Continued

| REAGENT or RESOURCE | SOURCE | IDENTIFIER |
|---|---|---|
| Experimental Models: Organisms/Strains | | |
| <i>D. melanogaster</i> : RNAi of dPiezo w; RNAi-Piezo8486R1/CyoWeep | National Institute of Genetics, Japan | NIG-RNAi stock number: 8486R-1 |
| <i>D. melanogaster</i> : RNAi of dPiezo: P{KK101815}VIE-260B | VDR Stock Center | VDR stock number: v105132; FlyBase: FBst0476960 |
| RNAi of dPiezo: w ¹¹¹⁸ ; P{GD993}v2796 | VDR Stock Center | VDR stock number: v2796; FlyBase: FBst0457216 |
| <i>D. melanogaster</i> : dPiezo KO: w*; PBac{RB5.WH5}Piezo ^{KO} | Bloomington <i>Drosophila</i> Stock Center | BDSC: 58770; FlyBase: FBst0058770 |
| <i>D. melanogaster</i> : dPiezo-Gal4: w*; P{Piezo-GAL4.1.0}III | Bloomington <i>Drosophila</i> Stock Center | BDSC: 59266; FlyBase: FBst0059266 |
| Mouse: NOD.Cg-Prkdc ^{scid} Il2rg ^{tm1Wjl} /SzJ (NSG) | The Jackson Laboratory | RRID: IMSR_JAX:005557 |
| Oligonucleotides | | |
| qPCR human <i>PIEZO1</i> forward primer:CTCTTCCTGGCGCTGTTC | This paper | N/A |
| qPCR human <i>PIEZO1</i> reverse primer:GATGAGGTTGGTGGAGTTGG | This paper | N/A |
| qPCR human <i>ACTB</i> forward primer:AGAGCTACGAGCTGCCTGAC | This paper | N/A |
| qPCR human <i>ACTB</i> reverse primer:AGCACTGTGTTGGCGTACAG | This paper | N/A |
| qPCR human <i>GAPDH</i> forward primer:CTCCTGCACCACTGCT | This paper | N/A |
| qPCR human <i>GAPDH</i> reverse primer:GGGCCATCCACAGTCTTCTG | This paper | N/A |
| Recombinant DNA | | |
| plasmid: pBMN(CMV-copGFP-Luc2-Puro) | Addgene | Plasmid #80389 |
| Plasmid: pLKO.1-shPIEZO1 #1 | Dharmacon | Clone ID: TRCN0000121969 |
| plasmid: pLKO.1-shPIEZO1 #2 | Dharmacon | Clone ID: TRCN0000142459 |
| plasmid: pTRIPZ-Tet-ON-shPIEZO1 #1 | Dharmacon | Clone ID: V3THS_361173 |
| plasmid: pTRIPZ-Tet-ON-shPIEZO1 #2 | Dharmacon | Clone ID: V3THS_361177 |
| Software and Algorithms | | |
| GraphPad Prism 5 | GraphPad Software | N/A |
| pClamp9 | Molecular Devices | N/A |
| MATLAB | MathWorks | N/A |
| Imaris | Bitplane | N/A |
| Volocity | Quorum Technologies | N/A |
| ImageJ | https://imagej.nih.gov/ij/ | N/A |
| Extreme Limiting Dilution Assay (ELDA) | http://bioinf.wehi.edu.au/software/elda/ | N/A |
| GSEA | http://software.broadinstitute.org/gsea/index.jsp | N/A |
| Kallisto | https://pachterlab.github.io/kallisto/ | N/A |
| DESeq2 | http://bioconductor.org/packages/release/bioc/html/DESeq2.html | N/A |
| G:Profiler | https://biit.cs.ut.ee/gprofiler/ | N/A |
| EnrichmentMap | http://www.baderlab.org/Software/EnrichmentMap | N/A |
| David | Laboratory of Human Retrovirology and Immunoinformatics | https://david.ncicfcr.gov/ |
| Cytoscape 3.6.1 | National Resource for Network Biology | http://www.cytoscape.org/ |

(Continued on next page)

Continued

| REAGENT or RESOURCE | SOURCE | IDENTIFIER |
|---------------------|--|---|
| HISAT2 | Center for Computational Biology, Johns Hopkins University | https://ccb.jhu.edu/software/hisat2/ |
| StringTie | Center for Computational Biology, Johns Hopkins University | https://ccb.jhu.edu/software/stringtie/ |
| VENNY2.1 | BioinfoGP | http://bioinfogp.cnb.csic.es/tools/venny/ |
| UpSetR | Gehlenborg Lab | https://gehlenborglab.shinyapps.io/upsetr/ |

CONTACT FOR REAGENT AND RESOURCE SHARING

Further information and requests for resources and reagents should be directed to and will be fulfilled by the Lead Contact, Xi Huang (xi.huang@sickkids.ca).

EXPERIMENTAL MODEL AND SUBJECT DETAILS***Drosophila* stocks**

Please refer to [Table S1](#) for the *Drosophila* stocks used in this study.

***Drosophila* study**

All larvae and flies were kept at 25°C unless otherwise specified. For experiments to study components of the integrin pathway ([Figures 3A and 3B](#)) and ECM rescue ([Figure S1B](#)) in dPiezo-deficient gliomas, room temperature (~22°C) was used. Randomly selected male and female larvae at the late third instar stage were studied.

Patient samples and cell culture

All samples were obtained following informed consent from patients. All experimental procedures were performed in accordance with the Research Ethics Board at The Hospital for Sick Children (Toronto, Canada). Approval to pathological data was obtained from the respective institutional review boards. Out of 8 patient samples, 3 were female and 5 were male, and ranged from 25- to 78-years of age. GS2, SF7225 and SF7881 GBM cell lines were cultured using DMEM with 10% FBS. GS2 cells have *RB* loss with methylated *MGMT* promoter. SF7225 cells have *PDGFR* amplification, p16 loss and unmethylated *MGMT* promoter. G508, G532 and G411 GBM stem cell lines, which were established from mesenchymal GBM tumors, were cultured using serum-free NS cell self-renewal media (NS media) consisted of Neurocult NS-A Basal media, supplemented with 2 mmol/L L-glutamine, hormone mix (in house equivalent to N2), B27 supplements, 75 µg/mL BSA, 2 µg/mL Heparin, 10 ng/mL basic FGF and 10 ng/mL human EGF. G508 cells display amplifications in *CDK4*, *MDM4*, *EGFR*, and loss of one copy of *PTEN*. G532 cells display amplification in *PDGFRA* and loss of one copy of *PTEN*. G411 cells display *EGFR* amplification, GBM stem cell lines were grown adherently on culture plates coated with poly-L-ornithine and laminin. All cell lines were regularly checked for mycoplasma infections and treated with Plasmodin (Invivogen) when infection was noted. No cell lines are listed in the database of commonly misidentified cell lines maintained by ICLAC and NCBI Biosample.

Mice

Eight weeks-old female NOD *scid* gamma /J#5557 immunodeficient mice were used for xenograft experiments. The mice were housed under aseptic conditions, which included filtered air and sterilized food, water, bedding, and cages. Age-matched mice with the same sex (female) were randomly assigned to experimental groups. All mice were subjected to stereotactic implantation of GBM stem cells. In the DOX treatment experiment, half of transplanted mice were fed with rodent diet containing 625 mg per kg of DOX which is estimated to provide 1.6-2.7 mg of DOX daily based on a 3-5 g diet. There were no specific inclusion or exclusion criteria. All procedures involving animals were performed in compliance with the Animals for Research Act of Ontario and the Guidelines of the Canadian Council on Animal Care. The Centre for Phenogenomics (TCP) Animal Care Committee reviewed and approved all procedures conducted on animals at TCP (protocol 19-0288H).

METHOD DETAILS***Drosophila* immunostaining, confocal microscopy and image quantifications**

3rd instar larvae were dissected in PBS, fixed in 4% formaldehyde for 20 min at room temperature, incubated with primary antibody overnight at 4°C and secondary antibody for 2 hours at room temperature. Primary antibodies include: mouse anti-Repo (1:60, DSHB), rabbit anti-phosphorylated Histone 3 (1:300, Abcam), Alexa Fluor 488 Phalloidin (1:40, Invitrogen), rabbit anti-phosphorylated

Fak (1:100, Thermo Fisher). Secondary antibodies conjugated to Alexa Fluor 488, 546 or 647 (Invitrogen) were used at 1: 500. Images were acquired with Leica SP8 confocal microscope.

For quantifying the volume of glial tissue or glioma, *repo-Gal4*-driven mRFP or eGFP was imaged and the tissue volume was determined by Imaris software after 3-D reconstruction of the z stack of confocal images. For quantifying the number of mitotic glia cells and total glia cells, Repo⁺; pHistone3⁺ and Repo⁺ cells in mRFP⁺ tumors were counted using the dot quantification analysis of Imaris, respectively. For quantifying Vkg-GFP, the signals were measured by Imaris in various defined volumes of 10⁵ μm³ mRFP⁺ tumors to generate volume and intensity values. For quantifying stress fibers, Phalloidin⁺ signal in mRFP⁺ tumors was measured by Imaris to generate the intensity value. All values were normalized to the average intensity of the control group. For quantifying phosphorylated Fak, pFak⁺ signal in mRFP⁺ tumors were measured by Imaris in various defined volumes of 10⁵ μm³ to generate the volume and intensity values.

Generating cell culture coverslips with various levels of stiffness, cell counting, self-renewal assay and immunofluorescence staining

Polyacrylamide (PA) gel substrates with different stiffness were fabricated on glass coverslips. Briefly, PA gel solutions were prepared by varying the concentration of acrylamide (3%–5%, Bio-Rad) and bis-acrylamide (0.01%–0.15%, Bio-Rad) in deionized water. Polymerization was initiated with 0.05% ammonium persulfate (Sigma) and 0.1% N,N,N',N'-Tetramethylethylenediamine (TEMED, Sigma). 15 μl of each final solution was pipetted onto the glass coverslips treated with 0.5% 3-aminopropyltrimethoxysilane (Sigma) and 1% glutaraldehyde (Sigma). To cross-link extracellular matrix protein onto PA gel surface, the gels were photoactivated by sulfosANPAH (Sigma) under UV light (10 min). Subsequently, gels were incubated in 200 μg/mL laminin solution (Sigma) at 37°C for 4 hours, followed by rinsing in phosphate buffered saline (PBS) and UV sterilization for 30 min. The Young's modulus (100 Pa, 500 Pa, 1 KPa or 5 KPa) of PA gels was quantified by AFM. For the cell counting experiment, same numbers of cells (10⁵ in each well of 6-well plate) were seeded for both the control and PIEZO1 knockdown groups at various stiffness conditions. From day 0 (seeding day) to day 6, images were acquired by the Nikon DS-L3 camera connected to a Nikon Eclipse TS100 inverted microscope with 10X objective lens. Cell numbers were quantified in five randomly selected imaging fields in three biological replicates. The specific PIEZO1 agonist Yoda1 was used at the concentration of 5 μM to activate the ion channel activity of endogenous PIEZO1.

To determine the clonogenic potential of GBM cells, cells were plated at clonal density (150 cells/mL of culture medium) into 60 mm plates. Cell colonies were stained with 0.05% crystal violet 7–10 days after seeding. Representative results from three independent experiments were shown for all clonogenic assays. For cell counting study, GBM stem cells were cultured adherently and in triplicates in 24-well plates. The cells were digested by Accutase for 5 min at 37°C, and the numbers of live cells were counted using Trypan Blue dye exclusion assay with Haemocytometer. Cell numbers were quantified by averaging the three biological replicates for each time point from day 2 to day 8. To perform stem cell sphere formation assay, GBM stem cells were plated in serial dilutions (ranging from 2000 to 3 cells per well) on non-adherent 96-well plates in six biological replicates. One week after plating, the numbers of wells with spheres were quantified and the data were analyzed by the Extreme Limiting Dilution Analysis (ELDA) software, which calculates the frequency of sphere forming cells and the differences between groups using the Chi-square test.

To perform immunofluorescence staining, GBM cells were fixed in 4% formaldehyde for 20 min at room temperature, incubated with primary antibody overnight at 4°C and secondary antibody for 2 hours at room temperature. The primary antibodies used were rabbit anti-PIEZO1 (1:400, Proteintech), mouse anti-activated β1 integrin (1:500, Abcam), mouse anti-Vinculin (1:1000, Millipore), mouse anti-FAK (1:400, BD Biosciences), mouse anti-Paxillin (1:400, BD Biosciences), and rabbit anti-phosphorylated Paxillin (Tyr118) (1:500, Invitrogen), and rabbit anti-Ki67 (1:3000, Abcam). Secondary antibodies conjugated to Alexa Fluor 488 or 546 (Invitrogen) were used at 1:1000. Images were acquired with Leica SP8 confocal microscope. The fluorescence intensity and size of focal adhesion and integrin-FAK signaling molecules were quantified by Volocity software. The intensity and puncta size of PIEZO1 at focal adhesion were quantified by PIEZO1 puncta signal at the site of focal adhesion molecules marked by β1 integrin.

Patient tissue staining and Microscopy

Tissue samples were fixed for 24 hours with PFA, paraffin embedded and serial sectioned. Sections were deparaffinized and rehydrated through an alcohol gradient to water for antigen retrieval in 10 mM citrate buffer PH 6.0 in a rice cooker. The rabbit anti-PIEZO1 antibody (1:200, Proteintech) was incubated overnight at 4°C, the anti-rabbit HRP step was done with 30-min incubation at room temperature. The DAB color reaction was developed at room temperature and stopped after 1 min. The slides were then counterstained with Hematoxylin. Tissue sections were imaged using 3DHistech Panoramic 250 Flash II Slide Scanner.

Real-Time Quantitative PCR

Total RNA from cells was isolated using PureLink™ RNA mini kit according to manufacturer's protocol (Thermo Fisher Scientific). cDNAs were synthesized with the Tetro reverse transcriptase (Bioline). Real-time PCR was performed using the following specific human primers: *PIEZO1* (forward: CTCTTCCTGGCGCTGTTTC; reverse: GATGAGGTTGGTGGAGTTGG); *ACTB* (forward: AGAGC TACGAGCTGCCTGAC; reverse: AGCACTGTGTTGGCGTACAG); *GAPDH* (forward, CTCCTGCACCACCACTGCT; reverse, GGGCCATCCACAGTCTTCTG). *ACTB* and *GAPDH* were used as internal controls for gene expression quantification. Real-time PCR was performed with ABI Vii7 using SYBR green PCR master mix. Relative mRNA abundance was done using the ΔΔCT method (in triplicates). Each experiment was performed in three biological replicates.

Lentivirus-mediated shRNA study

Human pLKO.1 lentiviral shRNA target gene set against *PIEZO1* and pLKO.1-TRC-control vector were obtained from Dharmacon. Virus infections were performed within antibiotics-free culture medium for 24 hours. *PIEZO1* shRNA mature antisense sequences are: #1: ATGATTGTA CTTCTTGGTGAG; #2: TTCCACCTGAATGTGGTCTTC.

Human pTRIPZ inducible lentiviral shRNA target gene set against *PIEZO1* vector were obtained from Dharmacon. Cells infected by virus were selected by Puromycin for 1 week. Cells were also screened for infection efficiency by calculating RFP positive cells after doxycycline induction. More than 95% of cells were infected. *PIEZO1* shRNA mature antisense sequences are: #1: TCTTCTGTCTCTCGGCT; #2: TGATGAAGTACTTGAGGCA.

Xenograft and *in vivo* bioluminescence imaging

Tumor cells with firefly-luciferase-expressing reporter

GBM cells were transduced with a lentiviral vector pBMN (CMV-copGFP-Luc2-Puro, Addgene plasmid #80389, a gift from Magnus Essand) containing GFP and firefly luciferase under the control of the cytomegalovirus (CMV) promoter. Cells were screened for infection efficiency by calculating GFP positive cells and by treatment with luciferin (D-luciferin potassium salt, Gold Biotechnology, St Louis, MO) *in vitro* and examination by the Xenogen IVIS Lumina System. More than 95% of cells were infected.

Surgical procedure for implantation of tumor cells

Eight weeks-old female *NOD scid gamma* /J#5557 immunodeficient mice were anesthetized using gaseous isoflurane and immobilized in a stereotaxic head frame. The skull of the mouse was exposed and a small opening was made using sterile dental drill (Precision Guide) at 2 mm lateral and 1 mm posterior to bregma. At this location, 10^5 G532 or G411 cells in 2 μ L Hanks' Balanced Salt Solution without Ca^{2+} and Mg^{2+} (HBSS) was slowly injected (over 3 min) 2.5 mm deep to the surface of the skull using a Hamilton syringe. All procedures were carried out under sterile conditions.

In vivo bioluminescence monitoring

In vivo bioluminescence imaging was performed using the Xenogen IVIS Lumina System coupled LivingImage software for data acquisition. Mice were anesthetized using gaseous isoflurane and imaged 10 min after intraperitoneal injection of luciferin. Signal intensity was quantified within a region of interest over the head defined by the LivingImage software.

Bioinformatics study

Datasets and Data processing

TCGA AffyU133a gene expression array data and IlluminaHiSeq RNA-seq data of LGGs and GBMs were downloaded from <https://tcga-data.nci.nih.gov/> via Xena Browser developed by UCSC. Clinical information and data of molecular biomarkers (IDH mutation, 1p/19q co-deletion, G-CIMP phenotype, MGMT promoter methylation and molecular subtype) were generated from TCGA publications. The clinical information and gene expression datasets of GEO: GSE16011, GSE4290, GSE4412, GSE43107 and GSE43378 were acquired from Gene Expression Omnibus (GEO). For GEO microarray datasets, background subtraction, normalization and expression summarization of raw CEL files were performed using the Robust Multi-array Average (RMA) algorithm in R and the Bioconductor package *affy*.

Determining *PIEZO1* correlated genes

The TCGA LGG-GBM RNA-seq dataset, TCGA LGG RNA-seq dataset, TCGA GBM RNA-seq dataset and TCGA u133a GBM dataset were processed to determine *PIEZO1* correlated genes. R package *psych* was used to calculate matrix correlations and probability of all the gene pairs in each dataset. Gene pairs with r value > 0.3 and False Discovery Rate (FDR) value < 0.05 were identified as significantly correlated. *PIEZO1* significantly correlated genes from each dataset were intersected according to correlation direction independently and the results were generated and visualized via a Venn diagram plotted by using the VENNY2.1 tool (<http://bioinfogp.cnb.csic.es/tools/venny/>). We regained matrixes of *PIEZO1*-related genes from 529 GBM (GBM u133a microarray) and 702 glioma (LGG-GBM RNA-seq). The hierarchical clustering with agglomerative average linkage targeting the new matrixes was performed using the R/ConsensusClusterPlus package.

Enrichment Analysis

For *PIEZO1* correlated genes, Gene Ontology (GO) enrichment analysis and Kyoto Encyclopedia of Genes and Genomes (KEGG) pathway analysis were performed using the DAVID 6.8 online tool. Background selection and gene list conversion were conducted. The molecular network of *PIEZO1* correlated genes and enriched pathways were generated using Cytoscape 3.6.1.

Survival Analysis

R package *survival* was used for overall survival analysis. Medians of *PIEZO1* expression in each dataset were used as primary cut-off point for log-rank test. For those datasets that can not be evaluated by *PIEZO1* medians, we used the widely accepted method, *cutoff finder*, to optimize the cutoff points. Cox proportional hazard (PH) model is executed by the function *Coxph* and *Survfit* from R packages. The best-scanned cutoff points are defined as the one with the most significant (log-rank test) split.

RNA-seq analysis

Transcript-level expression analysis of RNA-seq experiments was conducted following the "new Tuxedo" protocol established by Mihaela Pertea et al. HISAT2 was used for read alignments. StringTie was used for transcripts assembly and quantification. R package Ballgown was used for differential gene expression analysis. Differentially expressed genes with FDR < 0.05 and fold change > 2 (or < 0.5) were accepted as significant.

Determining high confidence *PIEZO1* target genes

UpSetR was used to identify high confidence *PIEZO1* target genes. Differentially expressed genes generated from RNA-seq and *PIEZO1* correlated genes based on TCGA datasets were analyzed. Those genes preserved after data filtering were identified as high confidence. The UpSetR Shiny Version can be acquired at <https://gehlenborglab.shinyapps.io/upsetr/>.

| Dataset | Platform | Data Source |
|------------------------------|------------------------------------|---|
| TCGA u133a GBM dataset | AffyU133a | https://tcga.xenahubs.net/download/TCGA.GBM.sampleMap/HT_HG-U133A.gz |
| TCGA GBM RNA-seq dataset | illuminaHiSeq | https://tcga.xenahubs.net/download/TCGA.GBM.sampleMap/HiSeqV2_exon.gz |
| TCGA LGG RNA-seq dataset | illuminaHiSeq | https://tcga.xenahubs.net/download/TCGA.LGG.sampleMap/HiSeqV2_exon.gz |
| TCGA LGG-GBM RNA-seq dataset | illuminaHiSeq | TCGA GBM RNA-seq dataset plus TCGA LGG RNA-seq dataset |
| GEO: GSE16011 | AffyU133p2.0 | https://www.ncbi.nlm.nih.gov/geo/download/?acc=GSE16011&format=file |
| GEO: GSE4290 | AffyU133p2.0 | https://www.ncbi.nlm.nih.gov/geo/download/?acc=GSE4290&format=file |
| GEO: GSE4412 | AffyU133a | https://www.ncbi.nlm.nih.gov/geo/download/?acc=GSE4412&format=file |
| GEO: GSE43107 | Affymetrix Human Exon 1.0 ST Array | https://www.ncbi.nlm.nih.gov/geo/download/?acc=GSE43107&format=file |
| GEO: GSE43378 | AffyU133p2.0 | https://www.ncbi.nlm.nih.gov/geo/download/?acc=GSE43378&format=file |

Firebrowse (<http://firebrowse.org>) was used to determine *PIEZO1* expression in multiple types of normal and tumors.

RNA-seq analysis of *PIEZO1* knockdown in G508 and G532 GBM cell lines

Paired-end reads were mapped to hg19 transcriptome, and transcript abundance was determined using Kallisto 0.43.0. Differential expression was determined using DESeq2. Dataset is available at GEO (GSE113261). Gprofiler was used to determine GO terms enriched in genes downregulated by more than 2-fold (adjusted $p < 0.05$) in both G508 and G532 upon *PIEZO1* knockdown. Visualization was generated using Cytoscape and EnrichmentMap, and manually annotated with appropriate phrases. Enrichment of specific GO terms were calculated using GSEA with the entire list of expressed genes preranked using signed P -value as metric.

PIEZO1 promoter methylation analysis

The TCGA lower grade glioma and glioblastoma multiforme (LGG-GBM) DNA methylation dataset was downloaded from Xenabrowser. This profile was measured by using the Illumina Infinium HumanMethylation450 platform. Beta values were generated at Johns Hopkins University and University of Southern California TCGA genome characterization center. The dataset can be downloaded from the following link: <https://tcga.xenahubs.net/download/TCGA.GBMLGG.sampleMap/HumanMethylation450.gz>. The probes are mapped onto human genome derived from GEO: GPL13534. Datasets of H3K4me3 ChIP-seq signal from IMR90, fetal adrenal gland, brain at fetal day 122, brain dorsal neocortex fetal, fetal heart, fetal intestine large, fetal intestine small, kidney at fetal day 122, lung at fetal day 122, fetal muscle trunk, fetal muscle leg, penis foreskin keratinocyte primary cells, penis foreskin fibroblast primary cells, penis foreskin melanocyte primary cells, fetal stomach and fetal thymus were downloaded and visualized by WASHU EPIGENOME BROWSER (<https://epigenomegateway.wustl.edu/>). Beta value of microarray probes spanning *PIEZO1* transcription start site were collected and normalized. Independent sample t test was used to compare the methylation status between IDH mutant and IDH wild-type gliomas.

Atomic force microscopy

Drosophila brains were dissected followed by incubation using DMEM. Next, the brains were immobilized to the surface of a 35 mm dish through spontaneous adhesion. The brains were examined using an atomic force microscopy (AFM, BioScope Catalyst, Bruker) mounted on an inverted microscope (Nikon Eclipse-Ti). AFM indentation tests were performed using a spherical tip (diameter: 30 μm) at different locations on the brains with a trigger force of 5 nN. Spherical tips were made by assembling a borosilicate glass microsphere onto a tipless AFM cantilever using epoxy glue. Cantilever spring constant was calibrated each time before experiment by measuring power spectral density of thermal noise fluctuation of the unladed cantilever. To determine the elastic modulus of brain tissue, a trigger force of 5 nN was applied. The area between indentation and retraction curves is negligible (Figure S1A) showing that the brain tissues behaved dominantly elastically. Therefore, Hertz model for a spherical tip was applied to fit the experimental indentation curves to calculate the elastic modulus. Data were analyzed using MATLAB (MathWorks) and the quantified data were graphed using GraphPad Prism.

Western blotting

Total proteins from samples were extracted using a lysis buffer containing 50mM HEPES, 150mM NaCl, 10% glycerol, 1mM EDTA, and 1% NP-40. Protease inhibitors cocktail (Pierce Prod# A32955) and 1mM dithiothreitol (DTT) were added into lysis buffer. All lysates were kept on ice for 20 min, then centrifuged at 4°C, 14,000 rpm for 10 min. 10 μg protein samples were resolved on

4%–12% Bis-Tris gel (Invitrogen #NW04125BOX) at 200 V for 20 min with MES running buffer. The proteins were then transferred onto PVDF membrane (Millipore #PVH0001) and blocked with 5% BSA and 0.1% Tween-20 in TBS. Western blot assays were performed using primary antibodies diluted in the blocking solution. Immunoreactive bands were visualized using Bio-Rad Chemidoc imaging system and analyzed using ImageJ software. The primary antibodies used were: rabbit anti-Piezo1 (Proteintech #15939-1-AP, 1:1000), mouse anti-FAK (BD Biosciences #610088, 1:1000), rabbit anti-pFAK (Tyr397) (Thermo Fisher #44624G, 1:1000), mouse anti- α tubulin (Sigma Aldrich, 1:5000), rabbit anti-GAPDH (New England Biolabs, 1:5000). Each experiment was performed in three or four biological replicates.

Generation of PIEZO1 deficient HEK293T clones

CRISPR-Cas9 mediated genome editing was used to generate PIEZO1 deficient HEK293T clones. Guide RNA 5'-GTGCAAG CAGTGTACGGCC-3' and 5'-AGCAGACTCTGCGTCGCGGT-3', targeting exon 6 and exon 7 of PIEZO1, respectively, were cloned into pX330-U6-Chimeric_BB-CBh-hSpCas9 (Addgene plasmid #42230, a gift from Feng Zhang). HEK293T cells were co-transfected in T25 flasks using 15 μ g of pX330 plasmid and 15 μ g of pBMN plasmid in 1.5 mL of OptiMEM (Life Technologies), combined with 40 μ L PolyEZ (BioMart) in 1.5 mL of OptiMEM. 3 days after transfection, single fluorescent cells were sorted into 96 well plates containing DMEM 10% FBS media using SH800 Cell Sorter (Sony Biotechnology). 12 colonies of each guide RNA transfected HEK293T cells were collected and PIEZO1 expression was assayed using western blot.

Electrophysiology

G532 GBM stem cells were seeded on laminin (5 μ g/mL overnight at 37°C)-coated plastic coverslips for 48–72 hours. Coverslips were transferred to a continuously perfused recording chamber. The perfusion solution consisted of (in mM) 140 NaCl, 5 KCl, 1.2 CaCl₂, 0.5 MgCl₂, 5 glucose, and 10 HEPES (pH adjusted to 7.3 with NaOH). Patch pipettes for recording, with resistance of 2–3 M Ω , were filled with intracellular solution consisting of (in mM) 140 CsCl, 1 EGTA, 10 HEPES, 4 ATP, and 0.1 GTP (pH adjusted to 7.3 with CsOH). Whole-cell currents at –80 mV were recorded using an Axopatch 700B amplifier (Molecular Devices). Pipettes for focal mechanical stimulation, with resistance of 0.7–1.5 M Ω , were filled with the extracellular-like solution consisting of (in mM) 130 NaCl, 10 HEPES, 10 TEA-Cl, 5 KCl, 1 CaCl₂, 1 MgCl₂ (pH adjusted to 7.3 with NaOH) with 300 sucrose (hypertonic solution) or without 300 sucrose (isotonic solution). The hypertonic high sucrose jet stream to the processes of the cell was used to evoke mechanosensitive currents via osmotic pressure-induced stretch of the cell membrane. 100 ms steps of positive pressure from 0 to 100 mmHg in 50 mmHg increments were applied to the stimulation electrode via Clampex-controlled high-speed pressure clamp system (HSPC-1; ALA-Scientific). The stimulation pipette was placed < 10 μ m from the stimulation site on the cell. 60 s inter-sweep-intervals allowed for recovery of any prolonged desensitized mechanically activated channels. A square glass perfusion barrel (0.4 mm in width) was positioned to deliver extracellular solution in the direction of the cell to ensure the pressure-driven hypertonic solution application could not accumulate around the cell. All experiments were performed at room temperature.

Data were acquired online, filtered at 4 kHz, digitized at 50 kHz, and analyzed offline using pClamp9 software (Molecular Devices). Analysis of mechanically activated currents by fold change was performed using peak currents from the onset of the pressure step to 1.0 s to account for any late or secondary currents. Quantified data were graphed using GraphPad Prism.

QUANTIFICATION AND STATISTICAL ANALYSIS

No statistical methods were used to pre-determine sample sizes. The statistical analyses were done afterward without interim data analysis. No data points were excluded. Two-tailed Student's *t* test was performed for comparison between two groups of samples. Two-Way ANOVA analyses were used to assess significance of multiple data points. The Kaplan–Meier estimator and GraphPad Prism software were used to generate survival curves. Differences between survival curves were calculated using a log-rank test. Data distribution was assumed to be normal but this was not formally tested. All data were collected and processed randomly. Each experiment was successfully reproduced at least three times and was performed on different days. The exact values of “*n*” (sample size) and the numbers of data points are provided in the figures and figure legends. All data are expressed as mean \pm SEM. We considered a *P* value less than 0.05 to be statistically significant.

DATA AND SOFTWARE AVAILABILITY

The accession number for the RNA-seq data reported in this paper is GEO: GSE113261.